# Soft Channel Estimation and Localization for Millimeter Wave Systems With Multiple Receivers

Xi Yang , Chao-Kai Wen , Senior Member, IEEE, Yu Han , Member, IEEE, Shi Jin , Senior Member, IEEE, and A. Lee Swindlehurst, Fellow, IEEE

Abstract—In millimeter wave (mmWave) communications, user position information can enable various position-based communication services, such as resource allocation, beam tracking and alignment, interference control, and synchronization. Classical localization methods focus on hard localization information, but soft localization provides the confidence levels in position estimates and thus enables the information to be efficiently fused with different measurements and application layers to realize integrated communication and localization. In this study, we propose a soft channel estimation and localization algorithm for an mmWave systems with multiple base stations. We present the Newtonized variational inference spectral estimation algorithm to extract soft information of position-related channel parameters. The soft localization algorithm estimates user position by using soft channel parameters from the expectation propagation simultaneous localization and mapping algorithm framework. The proposed algorithms realize channel estimation and localization in the communication process and refine the channel estimation through the localization information. Numerical results show that the proposed algorithms approach the Cramér-Rao lower bound for channel estimation and localization, and are thus verified to be effective.

Index Terms—Channel estimation, localization, mmWave system, soft information.

# I. INTRODUCTION

ILLIMETER wave (mmWave) technology plays a key role in fifth-generation mobile communication systems [1]. MmWave communication systems provide high data rates by exploiting the large bands of available spectra at

Manuscript received 16 August 2021; revised 19 February 2022 and 28 May 2022; accepted 2 July 2022. Date of publication 21 July 2022; date of current version 19 October 2022. The associate editor coordinating the review of this manuscript and approving it for publication was Prof. Sangarapillai Lambotharan. The work of Xi Yang, Yu Han, and Shi Jin was supported in part by the National Natural Science Foundation of China under Grants 61941104 and 61921004, in part by the Key Research and Development Program of Shandong Province under Grant 2020CXGC010108, and in part by the Fundamental Research Funds for the Central Universities under Grant 2242022k30005. The work of Chao-Kai Wen was supported in part by the Ministry of Science and Technology of Taiwan under Grant MOST 111-2221-E-110-020-MY3. (Corresponding author: Shi Jin.)

Xi Yang, Yu Han, and Shi Jin are with the National Mobile Communications Research Laboratory, Southeast University, Nanjing 210018, China (e-mail: yangxi@seu.edu.cn; hanyu@seu.edu.cn; jinshi@seu.edu.cn).

Chao-Kai Wen is with the Institute of Communications Engineering, National Sun Yat-sen University, Kaohsiung 804, Taiwan (e-mail: chaokai.wen@mail.nsysu.edu.tw).

A. Lee Swindlehurst is with the Center for Pervasive Communications and Computing, University of California, Irvine, CA 92697 USA (e-mail: swindle@uci.edu).

Digital Object Identifier 10.1109/TSP.2022.3192584

high frequencies [2]. MmWave technology is believed to have considerable potential for future mobile systems that integrate communication and localization [3], [4]. The wireless channels at mmWave frequencies usually comprise relatively fewer paths because of severe attenuation and reduced scattering. Communication between user and receivers relies heavily on line-of-sight (LoS) transmission. Position-related channel parameters, such as the angle-of-arrival (AoA) and delay of LoS paths, can be used to estimate user position. Extracting these parameters not only provides position information but also allows the estimation of channel state information (CSI) because the equivalent channels needed for communication services, such as detection and precoding, can be reconstructed using the channel structure. Obtaining accurate CSI and position information is crucial to enable future integrated communication systems [5] and reconfigurable intelligent surface-assisted systems [6], [7], [8], [9], [10], [11].

Channel estimation algorithms for mmWave systems have been discussed in many studies. The two types of methods that exploit structured channel models are grid-based and gridless methods [12]. Grid-based methods use a set of grid points to represent the possible values of channel parameters and search for feasible solutions. However, grid-based methods induce estimation bias, which decreases estimation performance. Gridless methods generally have better performance than grid-based methods because they treat channel parameters as continuous variables. An example of such methods is the sparse Bayesian learning for multipath channel estimation [13], [14]. Reference [15] investigated gridless channel estimation for mmWave systems by using atomic norm. In [16], the authors proposed the Newtonized orthogonal matching pursuit (NOMP) algorithm, which can be used in multipath channel estimation. However, these existing studies only provide hard estimates of channel parameters. Soft parameter estimates that include an indication of estimate quality are useful in a variety of communication services, especially localization applications. An example is the soft gridless algorithm in [17] that uses variational inference to provide soft frequency estimates in the form of von Mises distributions.

Localization methods can be classified into two main categories: direct and indirect localization [18], [19]. Direct localization uses the received waveform to estimate the user position directly [20], [21]. By contrast, indirect localization exploits estimated channel parameters for user positioning. Reference [22] studied sensor network localization and proposed a closed-form solution by using AoAs. In [23], the authors investigated

1053-587X © 2022 IEEE. Personal use is permitted, but republication/redistribution requires IEEE permission.

See https://www.ieee.org/publications/rights/index.html for more information.

localization with a single reference station by using a beam training approach. Localization for mmWave systems with weighted least squares methods was proposed in [24], [25], [26]. These existing studies only considered the localization problem and assumed that channel parameter estimates are already known at the receiver. Moreover, these studies only provided hard estimate decisions, that is, a single user position estimate. However, hard estimate decisions cannot satisfy the demands for extensive and flexible position-based services. In [27], [28], the authors introduce the terminology of soft positioning, which characterizes the spatial distribution of target position. References [29], [30] realizes the robust localization by exploiting the soft information of radio channels. In [31], [32], [33], [34], [35], the authors develop the BP-SLAM algorithm framework to systematically solve the soft localization and mapping problems by exploiting simultaneous localization and mapping (SLAM) techniques in a fully Bayesian manner. In [36], we proposed a general and fully Bayesian algorithm framework, that is, the expectation propagation simultaneous localization and mapping (EP-SLAM) algorithm framework, for soft localization with Gaussian distributions.

As mentioned previously, signal processing algorithms for joint channel estimation and localization are the foundation for integrated communication and localization services in future mmWave systems, and they are currently attracting extensive research interest. In [37], the authors revealed several potential uses of mmWave positioning in vehicular networks, such as automated driving in various forms. Beamwidth optimization and beam alignment for position-aware mmWave systems were investigated in [38] and [39], respectively. In general, possessing position information can significantly improve the performance of various communication services. In many applications, the confidence level in position estimate quality must also be determined to provide important context for estimates because localization algorithms provide different levels of performance in different propagation environments. If the soft information of position estimates is available, such as in the form of the spatial distribution of network user, then an appropriate strategy for subsequent decisions, such as vehicle speed control in automated driving, can be selected.

In the current study, we develop a soft channel estimation and localization algorithm for providing soft position information in mmWave systems. This work is a comprehensive extension of our conference version [40]. The main contributions of this study are as follows:

• We propose the Newtonized variational inference spectral estimation (NVISE) algorithm for a two-dimensional structured channel parameterized by AoA and delay. Similar to that proposed in [17], the NVISE algorithm solves the variational inference problem, but is uses a different approach. Specifically, NVISE uses a regular Newton method, similar to that in [16], to solve the problem, whereas the algorithm in reference [17] adopts an unnatural and complicated iterative method. Hence, unlike the algorithm in [17], the proposed NVISE algorithm can be easily extended to deal with high-dimensional problems for arbitrary beamforming designs, pilot signals, antenna

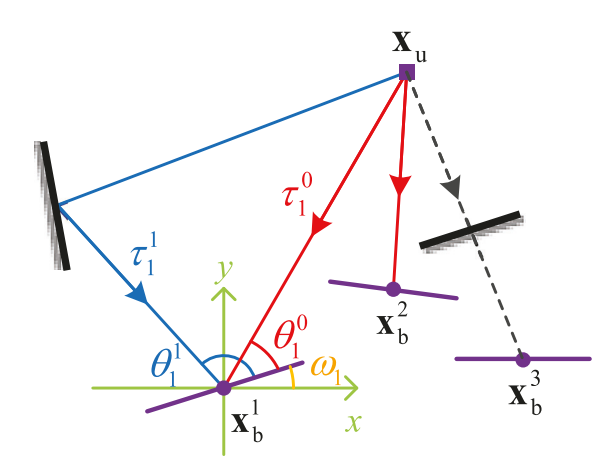


Fig. 1. Illustration of an mmWave system with three receivers.

array configurations, and hardware mechanisms, such as the mixed analog-to-digital converter (ADC) architecture in mmWave systems. More importantly, unlike that in [16] and other algorithms, NVISE extracts soft estimates of AoAs, delays, and complex channel gains that are characterized by a multivariate Gaussian distribution. This feature enables NVISE to achieve soft localization.

- The soft channel estimates provide confidence levels for the estimated parameters in different propagation environments. Leveraging the soft estimates of AoAs and delays, we propose soft localization algorithms for perfect and imperfect synchronization cases on the basis of the EP-SLAM algorithm framework. The proposed algorithms transfer the soft estimates of AoAs and delays to the soft user position in the form of a 2D Gaussian distribution. They also use the cost function to associate LoS paths and fuse the data accordingly.
- The performances of the proposed algorithms are investigated via simulations. Results show that the proposed algorithms approach the Cramér-Rao lower bound (CRLB) for channel estimation and localization parameters. The localization provides additional gains for channel estimation in the proposed integrated system. Moreover, the confidence levels for the soft user position information in indoor and outdoor scenarios are illustrated.

Notations: Capital and lowercase boldface letters denote matrices and vectors, respectively.  $\mathbf{A}^*, \mathbf{A}^T,$  and  $\mathbf{A}^H$  denote the conjugate, transpose, and conjugate transpose of  $\mathbf{A}$ , respectively;  $\mathrm{tr}(\mathbf{A})$  represents its trace.  $\mathbf{1}_M \in \mathbb{R}^{M \times 1}$  is the all-ones vector.  $\mathrm{E}\{\cdot\}$  denotes the expectation operator.  $\mathcal{D}_{\mathrm{KL}}(q(x)\|p(x)) = \int q(x) \ln \frac{q(x)}{p(x)} dx$  is the Kullback-Leibler (K-L) divergence between pdf q(x) and p(x).

#### II. SYSTEM MODEL

In this study, we consider an mmWave system with a single antenna user and several receivers. Each receiver is assumed to employ a uniform linear array (ULA) with M antennas, with an antenna spacing of  $\lambda/2$ , where  $\lambda$  is the carrier wavelength. The considered mmWave system uses orthogonal frequency

division multiplexing, with N subcarriers spaced by  $f_{\rm D}$  on the frequency axis. Fig. 1 shows an example with a user and three receivers located in different positions. The position of receiver 1 is expressed as  ${\bf x}_{\rm b}^1=(x_{\rm b}^1,y_{\rm b}^1)^T$ , and the corresponding rotation of its ULA is given by  $\omega_1$ . During the uplink training stage, the user transmits pilot signals, and the wireless signals arrive at each receiver along an LoS and several non-line-of-sight (NLoS) paths. Each path can be characterized by AoA and delay propagation parameters. For example,  $\theta_1^0$  and  $\tau_1^0$  are the AoA and delay of the LoS path of receiver 1, respectively.

In the frequency domain, the received signal at receiver i is given by

$$\mathbf{Y}_i = \mathbf{R}_i (\mathbf{H}_i \odot (\mathbf{1}_M \otimes \mathbf{x}^T) + \mathbf{W}_i), \tag{1}$$

where  $\mathbf{H}_i$  is defined as

$$\mathbf{H}_{i} = \sum_{k=0}^{K_{i}} g_{i}^{k} \mathbf{a} (\theta_{i}^{k}) \mathbf{b}^{T} (\tau_{i}^{k}). \tag{2}$$

In (1),  $\mathbf{R}_i \in \mathbb{C}^{M_r \times M}$  is the beamforming matrix with a radio frequency chain number  $M_r$ ,  $\mathbf{x} \in \mathbb{C}^{N \times 1}$  is the pilot signal, and  $\mathbf{W}_i \in \mathbb{C}^{M \times N}$  is the complex Gaussian noise with variance  $v_w$ . In addition,  $\odot$  and  $\otimes$  are the Hadamard and Kronecker products, respectively. The channel matrix  $\mathbf{H}_i \in \mathbb{C}^{M \times N}$  comprises an LoS path and  $K_i$  NLoS paths. The steering vectors  $\mathbf{a}(\theta_i^0) \in \mathbb{C}^{M \times 1}$  (for M antennas) and  $\mathbf{b}(\tau_i^0) \in \mathbb{C}^{N \times 1}$  (for N subcarriers) of the LoS path are expressed as

$$\mathbf{a}(\theta_i^0) = \left(1, e^{j\pi\cos(\theta_i^0)}, \dots, e^{j\pi(M-1)\cos(\theta_i^0)}\right)^T, \quad (3)$$

$$\mathbf{b}(\tau_i^0) = \left(1, e^{j2\pi f_D \tau_i^0}, \dots, e^{j2\pi (N-1)f_D \tau_i^0}\right)^T, \tag{4}$$

where  $\theta_i^0 \in (0,\pi)$  and  $\tau_i^0 \in (0,1/f_{\rm D})$  are the AoA and delay of the LoS path, respectively; and  $g_i^0$  is the corresponding complex channel coefficient. Similar definitions hold for  ${\bf a}(\theta_i^k), \, {\bf b}(\tau_i^k),$  and  $g_i^k$  of the NLoS path k (k>0). If the LoS path to one of the receivers is blocked by obstacles, then  $g_i^0 \simeq 0$ . For example, in Fig. 1 we see that the LoS path of receiver 3 is nonexistent.

Given the propagation parameters of the LoS path, the user position can be obtained using a topology condition. For receiver i, the user position  $\mathbf{x}_{\mathbf{u}} = (x_{\mathbf{u}}, y_{\mathbf{u}})^T$  is given by the following topology condition:

$$\begin{bmatrix} x_{\mathbf{u}} \\ y_{\mathbf{u}} \end{bmatrix} = \begin{bmatrix} x_{\mathbf{b}}^{i} \\ y_{\mathbf{b}}^{i} \end{bmatrix} + c\tau_{i}^{0} \begin{bmatrix} \cos(\theta_{i}^{0} + \omega_{i}) \\ \sin(\theta_{i}^{0} + \omega_{i}) \end{bmatrix}, \tag{5}$$

where c is the speed of light. Therefore, the user position estimate  $\hat{\mathbf{x}}_{\mathrm{u}} = (\hat{x}_{\mathrm{u}}, \hat{y}_{\mathrm{u}})^T$  can be computed using (5) with known receiver position  $\mathbf{x}_{\mathrm{b}}^i = (x_{\mathrm{b}}^i, y_{\mathrm{b}}^i)^T$  and ULA rotation  $\omega_i$  if the parameter estimates  $\hat{\theta}_i^0$  and  $\hat{\tau}_i^0$  of the LoS path are extracted from (1). A good user position estimate can be obtained by fusing the results of multiple receivers, such as receivers 1 and 2 in Fig. 1, according to the confidence levels of the results. In the proposed mmWave system, channel estimation and localization are achieved in the uplink training stage, where the channel estimate  $\hat{\mathbf{H}}_i$  is reconstructed using the estimates  $\hat{g}_i^k$ ,  $\hat{\theta}_i^k$ , and  $\hat{\tau}_i^k$  for each receiver, and the user is localized using the estimates  $\hat{\theta}_i^0$  and  $\hat{\tau}_i^0$  of the LoS paths.

Channel estimation and localization suffer from several problems. An appropriate channel estimation algorithm that can provide parameter estimates and their corresponding confidence levels is important for channel reconstruction and user localization. A systematic localization algorithm is needed to find the parameter estimates of the LoS paths among those of various NLoS paths and infer the user position jointly by using these parameter estimates. The localization algorithm must be capable of handling complex propagation environments (some LoS paths may be blocked) and the problems of missed detection and false alarms that arise from imperfect channel estimation.

The previous discussion assumes perfect synchronization among the user and receivers. However, a perfect synchronization is difficult to achieve over the air. For the imperfect synchronization case, the channel matrix of receiver i can be written as

$$\mathbf{H}_{i} = \sum_{k=0}^{K_{i}} g_{i}^{k} \mathbf{a} \left( \theta_{i}^{k} \right) \mathbf{b}^{T} \left( \tau_{i}^{k} + \tau_{u} \right), \tag{6}$$

where  $\tau_u$  is the clock bias. The receivers are synchronized through the wired network and thus share a common clock bias  $\tau_u$  caused by the synchronization error. For the imperfect synchronization case, the localization algorithm should be designed to simultaneously estimate the clock bias  $\tau_u$  and localize the user position  $\mathbf{x}_u$ .

The next section focuses on channel estimation. A general channel estimation algorithm, which is capable of providing soft parameter estimates for arbitrary steering vector forms and hardware platforms, is proposed on the basis of variational inference.

#### III. SOFT CHANNEL ESTIMATION

In this section, we develop a general channel estimation algorithm on basis of variational inference. The proposed NVISE algorithm can estimate the AoAs and delays in the families of multivariate Gaussian distributions, thus providing soft estimates of these parameters.

# A. Spectral Estimation Problem Formulation

NVISE is a general algorithm that can extract parameters by handling the measurement (received signal  $Y_i$ ) with an arbitrary posterior pdf. Therefore, for convenience, we consider the following simplified form of measurement:

$$\mathbf{Y} = \mathbf{H} + \mathbf{W} = \sum_{k=1}^{K} h_k e^{j\phi_k} \mathbf{a}(\theta_k) \mathbf{b}^T(\eta_k) + \mathbf{W}.$$
 (7)

In (7),  $\mathbf{W} \in \mathbb{C}^{M \times N}$  is complex Gaussian noise with variance  $v_w$ . The steering vectors  $\mathbf{a}(\theta_k) \in \mathbb{C}^{M \times 1}$  and  $\mathbf{b}(\eta_k) \in \mathbb{C}^{N \times 1}$  are defined as follows

$$\mathbf{a}(\theta_k) = \left(1, e^{j\pi\cos(\theta_k)}, \dots, e^{j\pi(M-1)\cos(\theta_k)}\right)^T, \quad (8)$$

$$\mathbf{b}(\eta_k) = \left(1, e^{j\eta_k}, \dots, e^{j(N-1)\eta_k}\right)^T. \tag{9}$$

The channel  $\mathbf{H} \in \mathbb{C}^{M \times N}$  comprises K components (paths), each of which is determined by  $(\theta_k, \eta_k, h_k, \phi_k)$ . For component  $k, \theta_k \in (0, \pi)$  represents the AoA, and  $\eta_k = 2\pi f_{\mathrm{D}} \tau_k \in (0, 2\pi)$  denotes the frequency associated with delay  $\tau_k$ . In addition,  $h_k e^{j\phi_k}$  is the complex channel coefficient, where  $h_k \in \mathbb{R}$  and  $\phi_k \in (0, 2\pi)$  are real numbers. The model order K and  $(\theta_k, \eta_k, h_k, \phi_k)$  of each component are unknown parameters that must be obtained from measurement  $\mathbf{Y}$ .

According to (7), one can use a factorized surrogate pdf such as  $q(\theta, \eta, \mathbf{h}, \phi) = q(\mathbf{h}, \phi) \prod_{k=1}^K q(\theta_k, \eta_k)$  to characterize  $(\theta_k, \eta_k, h_k, \phi_k)$  through the mean-field approximation and the variational inference [17], [41], [42], [43]. However, we consider a different approach, where the joint surrogate pdf  $q(\theta_k, \eta_k, h_k, \phi_k)$  is used to characterize each component. In particular,  $q(\theta_k, \eta_k, h_k, \phi_k)$  is restricted to the Gaussian distribution family, where the gradient descent method is used to refine the parameters of Gaussian pdf by maximizing the evidence lower bound (ELBO). In addition, the cyclic refinements are employed to incorporate the newly detected component by reevaluating the previously detected components.

First we focus on the single component case where K=1. The subscript k is omitted hereafter. A probabilistic model is used to characterize the problem through the posterior pdf:

$$p(\theta, \eta, h, \phi | \mathbf{Y}) = \frac{p(\mathbf{Y}, \theta, \eta, h, \phi)}{p(\mathbf{Y})},$$
(10)

where

$$p(\mathbf{Y}, \theta, \eta, h, \phi) = p(\theta)p(\eta)p(h)p(\phi)$$

$$\times \prod_{m=1}^{M} \prod_{n=1}^{N} f_{\text{CN}}\left(y_{mn}; he^{j\phi}e^{j(m-1)\pi\cos(\theta)}e^{j(n-1)\eta}, v_{w}\right), \tag{11}$$

and  $p(\mathbf{Y})$  is the marginal of the joint pdf (11) that acts as a normalizing constant. In (11),  $y_{mn}$  is the element in the m-th row and n-th column of  $\mathbf{Y} \in \mathbb{C}^{M \times N}$ , and  $f_{\mathrm{CN}}(x;m,v)$  represents the complex Gaussian distribution with mean m and variance v. If the prior information is unavailable, the uniform distributions are used to characterize the prior distributions  $p(\theta)$ ,  $p(\eta)$ , and  $p(\phi)$ . For example, we have  $p(\theta) = 1/\pi$ ,  $\theta \in (0,\pi)$ . Assuming that p(h) also follows a "uniform prior distribution," then  $p(\theta, \eta, h, \phi | \mathbf{Y})$  is given by

$$p(\theta, \eta, h, \phi | \mathbf{Y})$$

$$\propto \prod_{m=1}^{M} \prod_{n=1}^{N} f_{\rm CN}\Big(y_{mn}; he^{j\phi}e^{j(m-1)\pi\cos(\theta)}e^{j(n-1)\eta}, v_w\Big).$$
(12)

In fact, for the received signal (1) with deterministic beamforming matrix  $\mathbf{R}_i$  and pilot signal  $\mathbf{x}$ , we can obtain the corresponding posterior pdf  $p(\theta, \eta, h, \phi | \mathbf{Y}_i, \mathbf{R}_i, \mathbf{x})$  and solve it analogously by using the NVISE algorithm.

Equation (12) implies that the prior distribution (of  $\theta$ ,  $\eta$ , h, and  $\phi$ ) is not involved in the posterior pdf. References [41], [42], [43], [44], [45], [46], [47], [48], [49] uses the Bayesian hierarchical prior distribution to introduce sparsity. As shown in

Section III-C, the proposed algorithm introduces sparsity by sequentially extracting a few paths.

#### B. Variational Inference

According to the variational inference [50], for any surrogate pdf  $q(\theta, \eta, h, \phi)$ , the log model evidence can be obtained as:

$$\ln(p(\mathbf{Y})) = \mathcal{L}(q(\theta, \eta, h, \phi)) + \mathcal{D}_{KL}(q(\theta, \eta, h, \phi) || p(\theta, \eta, h, \phi || \mathbf{Y})), \quad (13)$$

where

$$\mathcal{L}(q(\theta, \eta, h, \phi)) = \mathbb{E}_{q(\theta, \eta, h, \phi)} \left\{ \ln \frac{p(\theta, \eta, h, \phi | \mathbf{Y})}{q(\theta, \eta, h, \phi)} \right\}. \tag{14}$$

Because the log model evidence is a constant, minimizing the K-L divergence between the posterior pdf (12) and the surrogate pdf  $q(\theta, \eta, h, \phi)$  is equivalent to maximizing ELBO  $\mathcal{L}(q(\theta, \eta, h, \phi))$  and tightening it as a lower bound to the log model evidence [17].

However, the posterior pdf (12) is intractable in general. Alternatively, we restrict the surrogate pdf to a certain family of pdf, and then use the tractable surrogate pdf to approximate the posterior pdf by maximizing ELBO. In this work, we use the multivariate (real) Gaussian distribution as the surrogate pdf:

$$q(\theta, \eta, h, \phi) = f_{\rm N}(\mathbf{s}; \hat{\mathbf{s}}, \hat{\mathbf{V}}),$$
 (15)

where  $\mathbf{s} = (\theta, \eta, h, \phi)^T$ ,  $\hat{\mathbf{s}} = (\hat{\theta}, \hat{\eta}, \hat{h}, \hat{\phi})^T$ , and  $\hat{\mathbf{V}}$  is given by

$$\hat{\mathbf{V}} = \begin{bmatrix}
\hat{v}_{\theta\theta} & \hat{v}_{\theta\eta} & \hat{v}_{\theta h} & \hat{v}_{\theta \phi} \\
\hat{v}_{\theta\eta} & \hat{v}_{\eta\eta} & \hat{v}_{\eta h} & \hat{v}_{\eta \phi} \\
\hat{v}_{\theta h} & \hat{v}_{\eta h} & \hat{v}_{h h} & \hat{v}_{h \phi} \\
\hat{v}_{\theta \phi} & \hat{v}_{\eta \phi} & \hat{v}_{h \phi} & \hat{v}_{\phi \phi}
\end{bmatrix}.$$
(16)

In (15),  $f_N(\mathbf{s}; \hat{\mathbf{s}}, \hat{\mathbf{V}})$  denotes the multivariate (real) Gaussian distribution, where  $\hat{\mathbf{s}}$  is the parameter estimate, and  $\hat{\mathbf{V}}$  is interpreted as the confidence level of the parameter estimates. Then we have

$$\mathcal{L}(q(\theta, \eta, h, \phi)) = \mathcal{E}_{q(\theta, \eta, h, \phi)} \{ \ln(p(\theta, \eta, h, \phi | \mathbf{Y})) \}. \tag{17}$$

The NVISE algorithm uses the Newton gradient descent method to maximize  $\mathcal{L}(q(\theta, \eta, h, \phi))$  by updating  $\hat{\mathbf{s}}$  and  $\hat{\mathbf{V}}$ . According to (12) and (17),  $\mathcal{L}(q(\theta, \eta, h, \phi))$  is given by

$$\mathcal{L}(q(\theta, \eta, h, \phi)) \simeq \mathbb{E}_{q(\theta, \eta, h, \phi)} \{ f(\theta, \eta, h, \phi) \},$$
 (18)

where

$$f(\theta, \eta, h, \phi) = \sum_{m=1}^{M} \sum_{n=1}^{N} \left[ \frac{2|y_{mn}|h}{v_w} \cos(\psi) - \frac{h^2}{v_w} \right], \quad (19)$$

in which

$$\psi = (m-1)\pi\cos(\theta) + (n-1)\eta + \phi - \angle y_{mn}.$$
 (20)

As a result of the characteristics of the spectral estimation problem,  $q(\theta, \eta, h, \phi) = f_{\rm N}(\mathbf{s}; \hat{\mathbf{s}}, \hat{\mathbf{V}})$  generally results in a covariance matrix  $\hat{\mathbf{V}}$  with small variances. Therefore,  $f(\theta, \eta, h, \phi)$  can be approximated as a linear function using first and second order derivatives.

For  $f(\theta, \eta, h, \phi)$ , the first-order derivatives at  $\mathbf{s} = \hat{\mathbf{s}}$  can be obtained as

$$d_{\theta} = \sum_{m=1}^{M} \sum_{n=1}^{N} \frac{2|y_{mn}| h}{v_{w}} (m-1) \sin(\psi) \pi \sin(\theta), \qquad (21a)$$

$$d_{\eta} = \sum_{m=1}^{M} \sum_{n=1}^{N} -\frac{2|y_{mn}|h}{v_w} (n-1)\sin(\psi), \tag{21b}$$

$$d_h = \sum_{m=1}^{M} \sum_{n=1}^{N} \frac{2|y_{mn}|}{v_w} \cos(\psi) - \frac{2 \ hMN}{v_w}, \tag{21c}$$

$$d_{\phi} = \sum_{m=1}^{M} \sum_{n=1}^{N} -\frac{2|y_{mn}| h}{v_w} \sin(\psi).$$
 (21d)

In addition, the second-order derivatives at  $s = \hat{s}$  are given by

$$a_{\theta\theta} = \sum_{m=1}^{M} \sum_{n=1}^{N} \frac{2|y_{mn}| h}{v_w} [(m-1)\sin(\psi)\pi\cos(\theta) - (m-1)^2\cos(\psi)\pi^2\sin^2(\theta)], \qquad (22a)$$

$$a_{\theta\eta} = \sum_{m=1}^{M} \sum_{n=1}^{N} \frac{2|y_{mn}| h}{v_w} (m-1)(n-1)\cos(\psi)\pi\sin(\theta),$$
(22b)

$$a_{\theta h} = \sum_{m=1}^{M} \sum_{n=1}^{N} \frac{2|y_{mn}|}{v_w} (m-1)\sin(\psi)\pi\sin(\theta),$$
 (22c)

$$a_{\theta\phi} = \sum_{m=1}^{M} \sum_{n=1}^{N} \frac{2|y_{mn}| h}{v_w} (m-1)\cos(\psi)\pi\sin(\theta), \quad (22d)$$

$$a_{\eta\eta} = \sum_{m=1}^{M} \sum_{n=1}^{N} -\frac{2|y_{mn}| h}{v_w} (n-1)^2 \cos(\psi), \tag{22e}$$

$$a_{\eta h} = \sum_{m=1}^{M} \sum_{n=1}^{N} -\frac{2|y_{mn}|}{v_w} (n-1)\sin(\psi), \qquad (22f)$$

$$a_{\eta\phi} = \sum_{m=1}^{M} \sum_{n=1}^{N} -\frac{2|y_{mn}| h}{v_w} (n-1)\cos(\psi), \tag{22g}$$

$$a_{hh} = -\frac{2 MN}{v_w},\tag{22h}$$

$$a_{h\phi} = \sum_{m=1}^{M} \sum_{n=1}^{N} -\frac{2|y_{mn}|}{v_w} \sin(\psi), \tag{22i}$$

$$a_{\phi\phi} = \sum_{m=1}^{M} \sum_{n=1}^{N} -\frac{2|y_{mn}| h}{v_w} \cos(\psi). \tag{22j}$$

According to (18), (19), (21), and (21),  $\mathcal{L}(q(\theta, \eta, h, \phi))$  can be approximated as

$$\begin{split} \mathcal{L}(q(\theta,\eta,h,\phi)) &\simeq f(\hat{\theta},\hat{\eta},\hat{h},\hat{\phi}) + \frac{\hat{a}_{\theta\theta}\hat{v}_{\theta\theta}}{2} + \frac{\hat{a}_{\eta\eta}\hat{v}_{\eta\eta}}{2} + \frac{\hat{a}_{hh}\hat{v}_{hh}}{2} & \text{on the set of grid points of} \\ &+ \frac{\hat{a}_{\phi\phi}\hat{v}_{\phi\phi}}{2} + \hat{a}_{\theta\eta}\hat{v}_{\theta\eta} + \hat{a}_{\theta h}\hat{v}_{\theta h} + \hat{a}_{\theta\phi}\hat{v}_{\theta\phi} & \Omega = \left\{ \left( \frac{2\pi k_1}{M\gamma_M}, \frac{2\pi k_2}{N\gamma_N} \right), \right. \end{split}$$

$$+\hat{a}_{\eta h}\hat{v}_{\eta h} + \hat{a}_{\eta \phi}\hat{v}_{\eta \phi} + \hat{a}_{h \phi}\hat{v}_{h \phi}. \tag{23}$$

In (23),  $\hat{a}_{\theta\theta}$  is given by

$$\hat{a}_{\theta\theta} = a_{\theta\theta}|_{\theta = \hat{\theta}, \eta = \hat{\eta}, h = \hat{h}, \phi = \hat{\phi}}, \tag{24}$$

where  $a_{\theta\theta}$  is defined in (22a). The other parameters in (23), such as  $\hat{a}_{\theta\phi}$ , follow similar definitions.

According to (23), the maximization of  $\mathcal{L}(q(\theta, \eta, h, \phi))$  can be achieved by iteratively updating  $\hat{s}$  and  $\hat{V}$  through the Newton gradient descent method. However, updating s and V simultaneously requires high computational complexity. A subspace update approach, where  $\hat{\mathbf{s}}$  and  $\hat{\mathbf{V}}$  are updated sequentially, is considered instead. For example, according to (23),  $\mathcal{L}(q(\theta, \eta, h, \phi)) = f(\hat{\theta}, \hat{\eta}, \hat{h}, \hat{\phi})$  when  $\hat{\mathbf{V}} = \mathbf{0}$ . The local maximum of  $\mathcal{L}(q(\theta, \eta, h, \phi))$  around  $\mathbf{s} = \hat{\mathbf{s}}$  can be obtained by updating s through the Newton gradient descent update

$$\hat{\mathbf{s}} \leftarrow \hat{\mathbf{s}} - \hat{\mathbf{A}}^{-1} \hat{\mathbf{d}},\tag{25}$$

where

$$\hat{\mathbf{A}} = \begin{bmatrix} \hat{a}_{\theta\theta} & \hat{a}_{\theta\eta} & \hat{a}_{\theta h} & \hat{a}_{\theta\phi} \\ \hat{a}_{\theta\eta} & \hat{a}_{\eta\eta} & \hat{a}_{\eta h} & \hat{a}_{\eta\phi} \\ \hat{a}_{\theta h} & \hat{a}_{\eta h} & \hat{a}_{h h} & \hat{a}_{h\phi} \\ \hat{a}_{\theta\phi} & \hat{a}_{\eta\phi} & \hat{a}_{h\phi} & \hat{a}_{\phi\phi} \end{bmatrix}, \tag{26}$$

$$\hat{\mathbf{d}} = \left(\hat{d}_{\theta}, \hat{d}_{\eta}, \hat{d}_{h}, \hat{d}_{\phi}\right)^{T}.$$
(27)

In (27),  $\hat{d}_{\theta}$  is given by

$$\hat{d}_{\theta} = d_{\theta}|_{\theta = \hat{\theta}, \eta = \hat{\eta}, h = \hat{h}, \phi = \hat{\phi}}, \tag{28}$$

where  $d_{\theta}$  is defined as (21a). In addition,  $\hat{d}_{\eta}$ ,  $\hat{d}_{h}$ , and  $\hat{d}_{\phi}$  follow similar definitions. As the multivariate Gaussian distribution (15) is used to approximate the posterior pdf (12), after the update of  $\hat{s}$  in (25),  $\hat{V}$  can be updated using the following local second-order gradient:

$$\hat{\mathbf{V}} \leftarrow -\hat{\mathbf{A}}^{-1}.\tag{29}$$

In (29),  $\hat{\mathbf{A}}$  is recomputed using the updated  $\hat{\mathbf{s}}$  that was obtained from (25). Given arbitrary and fixed  $\hat{\mathbf{V}}$ , the Newton gradient decent updates can be obtained similarly using (23) rather than  $\mathcal{L}(q(\theta, \eta, h, \phi)) = f(\hat{\theta}, \hat{\eta}, h, \phi)$ . Given space limitations, the computational details are omitted herein.

#### C. NVISE Algorithm

In the previous analysis, variational inference with Newton gradient descent updates is derived for the single component case with K=1. The Newton gradient descent update requires the initialization of  $\hat{\mathbf{s}}$  and  $\hat{\mathbf{V}}$ . We propose to use the orthogonal matching pursuit (OMP) algorithm to initialize s. The OMP algorithm extracts the component from the measurement by maximizing the following function:

$$(\hat{\theta}, \hat{\eta}) = \underset{(\theta, \eta) \in \Omega}{\arg \max} \left| \mathbf{a}^{H}(\theta) \mathbf{Y} \mathbf{b}^{*}(\eta) \right|^{2}$$
(30)

on the set of grid points of

$$\Omega = \left\{ \left( \frac{2\pi k_1}{M\gamma_M}, \frac{2\pi k_2}{N\gamma_N} \right) \right\}$$

$$k_1 = 0, 1, \dots, M\gamma_M - 1, k_2 = 0, 1, \dots, N\gamma_N - 1\},$$
 (31)

where the integers  $\gamma_M>1$  and  $\gamma_N>1$  are oversampling rates. The corresponding least squares estimate of the channel coefficient is given by

$$\hat{h}e^{j\hat{\phi}} = \frac{1}{NM}\mathbf{a}^{H}(\hat{\theta})\mathbf{Y}\mathbf{b}^{*}(\hat{\eta}). \tag{32}$$

Our proposed NVISE approach is summarized in Algorithm 1. NVISE sequentially extracts the components from the measurement. Before the extraction of a new component, the extracted components are refined through several rounds of single and cyclic Newton refinements (gradient descent updates).

Assume that l-1 components characterized by  $\hat{\mathbf{s}}_k$  and  $\hat{\mathbf{V}}_k$  with  $k=1,2,\cdots,l-1$  have been extracted. The residual measurement is given by

$$\mathbf{Y}_{r} = \mathbf{Y} - \sum_{k=1}^{l-1} \hat{h}_{k} e^{j\hat{\phi}_{k}} \mathbf{a}(\hat{\theta}_{k}) \mathbf{b}^{T}(\hat{\eta}_{k}). \tag{33}$$

In Algorithm 1, a new component characterized by  $\hat{\mathbf{s}}_l = (\hat{\theta}_l, \hat{\eta}_l, \hat{h}_l, \hat{\phi}_l)^T$  is initialized in line 2 by using  $\mathbf{Y}_r$  rather than  $\mathbf{Y}$ . In addition,  $\hat{\mathbf{V}}_l = \mathbf{0}$  is initialized.

Then,  $R_s$  rounds of Newton gradient descent updates are performed for component l with  $\hat{\mathbf{s}}_l$  and  $\hat{\mathbf{V}}_l$  in line 3. Given fixed  $(\hat{\mathbf{s}}_k, \hat{\mathbf{V}}_k), k = 1, 2, \dots, l-1$ , the posterior pdf is

$$p(\theta_l, \eta_l, h_l, \phi_l | \mathbf{Y})$$

$$\simeq \prod_{m=1}^{M} \prod_{n=1}^{N} f_{\text{CN}} \left( y_{mn}; \psi + h_l e^{j\phi_l} e^{j(m-1)\pi\cos(\theta_l)} e^{j(n-1)\eta_l}, v_w \right)$$

$$= \prod_{m=1}^{M} \prod_{n=1}^{N} f_{\text{CN}} \Big( y_{mn} - \psi; h_l e^{j\phi_l} e^{j(m-1)\pi\cos(\theta_l)} e^{j(n-1)\eta_l}, v_w \Big),$$
(34)

where

$$\psi = \sum_{k=1}^{l-1} \hat{h}_k e^{j\hat{\phi}_k} e^{j(m-1)\pi\cos(\hat{\theta}_k)} e^{j(n-1)\hat{\eta}_k}.$$
 (35)

Therefore, the Newton gradient descent update with posterior pdf (34) can be performed similar to the approach discussed in Section III-B. Note that the components  $1, 2, \dots, l-1$  are fixed when updating  $\hat{\mathbf{s}}_l$  and  $\hat{\mathbf{V}}_l$  for component l.

Next,  $R_c$  rounds of cyclic Newton gradient descent updates are performed for components  $1, 2, \dots, l$  in line 4 to minimize the K-L divergence for l components rather than for a single component with K=1. In each round, the Newton gradient descent updates are performed for component  $1 \to 2 \to \cdots \to l$  sequentially. For component i, the posterior pdf is given by

$$p(\theta_i, \eta_i, h_i, \phi_i | \mathbf{Y})$$

$$\simeq \prod_{m=1}^{M} \prod_{n=1}^{N} f_{\text{CN}} \Big( y_{mn} - \psi; h_i e^{j\phi_i} e^{j(m-1)\pi\cos(\theta_i)} e^{j(n-1)\eta_i}, v_w \Big),$$
(36)

# Algorithm 1: NVISE Algorithm.

**Input:** Measurement  $\mathbf{Y}$ , Newton refinement steps  $R_s$  and  $R_c$ .

Initialization: l = 0.

while l < L

- $1: l \leftarrow l + 1,$
- 2: Perform grid detection to initialize  $\hat{\mathbf{s}}_l$  and  $\hat{\mathbf{V}}_l$ ,
- 3: Perform  $R_s$  rounds of single Newton refinements on  $\hat{\mathbf{s}}_l$  and  $\hat{\mathbf{V}}_l$ ,
- 4: Update:  $R_c$  rounds of cyclic Newton refinements on  $(\hat{\mathbf{s}}_1, \hat{\mathbf{V}}_1) \to (\hat{\mathbf{s}}_2, \hat{\mathbf{V}}_2) \to \cdots \to (\hat{\mathbf{s}}_l, \hat{\mathbf{V}}_l)$ .

end

**Output:**  $(\hat{\mathbf{s}}_k, \hat{\mathbf{V}}_k), k = 1, 2, \dots, L.$ 

where

$$\psi = \sum_{k=1, k \neq i}^{l} \hat{h}_k e^{j\hat{\phi}_k} e^{j(m-1)\pi\cos(\hat{\theta}_k)} e^{j(n-1)\hat{\eta}_k}.$$
 (37)

The Newton gradient descent update for component i can be obtained analogously. Unlike the single Newton refinement, the cyclic Newton refinement completes the minimization of the K-L divergence for all l components.

The NVISE algorithm repeats the above procedures until L components are extracted from the measurement. The channel matrix is then reconstructed as follows:

$$\hat{\mathbf{H}} = \sum_{k=1}^{L} \hat{h}_k e^{j\hat{\phi}_k} \mathbf{a}(\hat{\theta}_k) \mathbf{b}^T(\hat{\eta}_k). \tag{38}$$

In addition, the covariance matrix  $\hat{\mathbf{V}}_k$  indicates the confidence level of  $(\phi_k, \eta_k), k = 1, 2, \cdots, L$ , which enables the soft localization algorithm. Furthermore, the following constant false alarm rate based termination criterion can be used similar to that in [16]: NVISE will stop if the power of the residual measurement (33) is lower than a threshold. NVISE may miss some components when L < K, but it may extract spurious components when L > K. The missed detection and false alarm problems will be addressed in the soft localization. In addition, there are other promising approaches, such as the soft thresholds provided by the sparsity enforcing hierarchical models [17], [41], [42], [43], [51], [52], [53].

A simplified version of NVISE can be obtained by assuming the steering vectors are approximately orthogonal. In the simplified version, the Newton gradient descent update is performed for  $(\theta, \eta)$  with a fixed complex channel coefficient  $\hat{g} = \hat{h}e^{j\hat{\phi}}$  rather than  $(\theta, \eta, h, \phi)$ . The details of the Newton gradient descent update for the simplified algorithm can be obtained in the same way as detailed above. In addition, after any Newton gradient descent update in lines 3 and 4, the complex channel coefficient is updated using the least squares estimation:

$$\hat{g}_i = \mathbf{a}^H(\hat{\theta}_i) \frac{\mathbf{Y} - \sum_{k=1, k \neq i}^l \hat{g}_k \mathbf{a}(\hat{\theta}_k) \mathbf{b}^T(\hat{\eta}_k)}{NM} \mathbf{b}^*(\hat{\eta}_i).$$
(39)

*Remark 1:* Similar to the NOMP algorithm, the NVISE algorithm uses the Newton method to solve the spectral estimation

problem [16]. However, NVISE considers the general K-L divergence minimization cost function in the Bayesian perspective. Meanwhile, the NOMP algorithm can be viewed as a special case of NVISE with linear observation with complex Gaussian noise and  $\hat{\mathbf{V}} = \mathbf{0}$ . Therefore, NOMP cannot handle nonlinear observations with an arbitrary form of noise and is unable to provide soft information (confidence level) of the parameter estimate  $\hat{\mathbf{s}}$ . In soft localization algorithms, soft information is indispensable.

#### D. Generation

NVISE is a general algorithm that is capable of handling arbitrary posterior pdfs for the spectral estimation problems. Hence, NVISE can be applied to different cases for the considered system, such as antenna arrays without a uniform configuration and users with multiple antennas. In addition, because of the prohibitive cost and power consumption of high-resolution ADCs, practical mmWave system systems often adopt mixed ADC architectures [2]. For example, the quantized signal at the *m*-th antenna and *n*-th subcarrier is given by

$$z_{mn} = \mathcal{Q}\left(\sum_{k=1}^{K} h_k e^{j\phi_k} e^{j(m-1)\pi\cos(\theta_k)} e^{j2\pi(n-1)f_D\tau_k} + w_{mn}\right),$$
(40)

where  $w_{mn}$  is complex Gaussian noise and  $\mathcal{Q}(\cdot)$  is the quantization function [54]. Similarly, NVISE can handle posterior pdfs that characterize quantized signals (40) using similar techniques. However, the above extensions are beyond the scope of this study.

#### IV. SOFT LOCALIZATION

In this section, we propose a soft localization algorithm for the considered mmWave system on the basis of the EP-SLAM algorithm framework [36]. The EP-SLAM algorithm framework provides a systematic and fully Bayesian solution for localization and mapping problems. In Section IV-A, a soft user position estimate is derived using the soft parameter estimates obtained from the NVISE algorithm. Soft localization algorithms for perfect and imperfect synchronization cases are proposed in Sections IV-B and IV-C, respectively.

#### A. Soft User Position

Given the propagation parameter estimates  $\hat{\theta}$  and  $\hat{\eta}$  and the confidence levels  $\hat{v}_{\theta\theta}$ ,  $\hat{v}_{\theta\eta}$ , and  $\hat{v}_{\eta\eta}$ , user position can be computed using topology condition (5). According to (5) and  $\eta = 2\pi f_{\rm D} \tau$ , given  $\theta = \hat{\theta}$  and  $\eta = \hat{\eta}$ , user position estimate  $\hat{\mathbf{x}}_{\rm u}$  can be obtained as

$$\begin{bmatrix} \hat{x}_{\mathbf{u}} \\ \hat{y}_{\mathbf{u}} \end{bmatrix} = \begin{bmatrix} x_{\mathbf{b}}^{i} \\ y_{\mathbf{b}}^{i} \end{bmatrix} + \frac{c\hat{\eta}}{2\pi f_{\mathbf{D}}} \begin{bmatrix} \cos(\hat{\theta} + \omega_{i}) \\ \sin(\hat{\theta} + \omega_{i}) \end{bmatrix}. \tag{41}$$

The confidence level of  $\hat{\mathbf{x}}_u$  needs to be determined to find the LoS paths and fuse the user position estimates of all receivers. In the following analysis, the confidence level of  $\hat{\mathbf{x}}_u$  is measured through first-order approximations.

Differentiation with respect to  $\theta$  and  $\eta$  on the two sides of (5) at  $(\hat{\theta}, \hat{\eta})$  yields the first-order approximations

$$\Delta_{x_{\rm u}} = -\frac{c\hat{\eta}}{2\pi f_{\rm D}} \sin(\hat{\theta} + \omega_i) \Delta_{\theta} + \frac{c}{2\pi f_{\rm D}} \cos(\hat{\theta} + \omega_i) \Delta_{\eta},$$
(42a)

$$\Delta_{y_{\rm u}} = \frac{c\hat{\eta}}{2\pi f_{\rm D}}\cos(\hat{\theta} + \omega_i)\Delta_{\theta} + \frac{c}{2\pi f_{\rm D}}\sin(\hat{\theta} + \omega_i)\Delta_{\eta}. \tag{42b}$$

According to the NVISE algorithm,  $\Delta_{\theta}$  and  $\Delta_{\eta}$  follow multivariate Gaussian distribution with the following covariance matrix:

$$\hat{\mathbf{V}} = \begin{bmatrix} \hat{v}_{\theta\theta} & \hat{v}_{\theta\eta} \\ \hat{v}_{\theta\eta} & \hat{v}_{\eta\eta} \end{bmatrix}. \tag{43}$$

On the basis of (42a) and (43), the variance of  $\Delta_{x_{\rm u}}$  can be obtained as

$$\hat{v}_{x_{u}x_{u}} = \frac{c^{2}\hat{\eta}^{2}}{4\pi^{2}f_{D}^{2}}\sin^{2}(\hat{\theta} + \omega_{i})\hat{v}_{\theta\theta} + \frac{c^{2}}{4\pi^{2}f_{D}^{2}}\cos^{2}(\hat{\theta} + \omega_{i})\hat{v}_{\eta\eta} - \frac{c^{2}\hat{\eta}}{2\pi^{2}f_{D}^{2}}\sin(\hat{\theta} + \omega_{i})\cos(\hat{\theta} + \omega_{i})\hat{v}_{\theta\eta}.$$
(44)

Similarly, the variance of  $\Delta_{y_n}$  is given by

$$\hat{v}_{y_{u}y_{u}} = \frac{c^{2}\hat{\eta}^{2}}{4\pi^{2}f_{D}^{2}}\cos^{2}(\hat{\theta} + \omega_{i})\hat{v}_{\theta\theta} + \frac{c^{2}}{4\pi^{2}f_{D}^{2}}\sin^{2}(\hat{\theta} + \omega_{i})\hat{v}_{\eta\eta} + \frac{c^{2}\hat{\eta}}{2\pi^{2}f_{D}^{2}}\sin(\hat{\theta} + \omega_{i})\cos(\hat{\theta} + \omega_{i})\hat{v}_{\theta\eta}.$$
(45)

In addition, the covariance between  $\Delta_{x_u}$  and  $\Delta_{y_u}$  follows

$$\hat{v}_{x_{\mathbf{u}}y_{\mathbf{u}}} = \frac{c^2}{4\pi^2 f_{\mathbf{D}}^2} \sin(\hat{\theta} + \omega_i) \cos(\hat{\theta} + \omega_i) \left(-\hat{\eta}^2 \hat{v}_{\theta\theta} + \hat{v}_{\eta\eta}\right) + \frac{c^2 \hat{\eta}}{4\pi^2 f_{\mathbf{D}}^2} \left(-\sin^2(\hat{\theta} + \omega_i) + \cos^2(\hat{\theta} + \omega_i)\right) \hat{v}_{\theta\eta}.$$
(46)

Therefore, the covariance matrix that characterizes the confidence level of  $\hat{\mathbf{x}}_u$  can be expressed as

$$\hat{\mathbf{V}}_{\mathbf{u}} = \begin{bmatrix} \hat{v}_{x_{\mathbf{u}}x_{\mathbf{u}}} & \hat{v}_{x_{\mathbf{u}}y_{\mathbf{u}}} \\ \hat{v}_{x_{\mathbf{u}}y_{\mathbf{u}}} & \hat{v}_{y_{\mathbf{u}}y_{\mathbf{u}}} \end{bmatrix}. \tag{47}$$

According to the analysis, user position estimates can be characterized by a 2D Gaussian distribution  $f_N(\hat{\mathbf{x}}_u, \hat{\mathbf{V}}_u)$ , where  $\hat{\mathbf{x}}_u$  and  $\hat{\mathbf{V}}_u$  are defined as (41) and (47), respectively. Note that the above computation rules only apply to the LoS path.

## B. Perfect Synchronization Case

In this part, we propose a soft localization algorithm based on the EP-SLAM algorithm framework. Two problems emerge in user localization: 1) data association to find the LoS path among the NLoS paths for each receiver and 2) data fusion to fuse the user position estimates provided by the LoS paths of all receivers.

Data fusion problem can be solved by exploiting the Gaussian reproduction formula [50]

$$f_{\rm N}(\hat{\mathbf{x}}_{\rm a}, \hat{\mathbf{V}}_{\rm a}) f_{\rm N}(\hat{\mathbf{x}}_{\rm b}, \hat{\mathbf{V}}_{\rm b}) = C f_{\rm N}(\hat{\mathbf{x}}_{\rm c}, \hat{\mathbf{V}}_{\rm c}),$$
 (48)

where C is a constant and

$$\hat{\mathbf{x}}_{c} = \hat{\mathbf{V}}_{c} \Big( \hat{\mathbf{V}}_{a}^{-1} \hat{\mathbf{x}}_{a} + \hat{\mathbf{V}}_{b}^{-1} \hat{\mathbf{x}}_{b} \Big), \tag{49a}$$

$$\hat{\mathbf{V}}_{c} = \left(\hat{\mathbf{V}}_{a}^{-1} + \hat{\mathbf{V}}_{b}^{-1}\right)^{-1}.$$
 (49b)

In soft localization, mapping, and tracking, the probabilistic association methods are usually used to solve data association problems [29], [30], [55], [56]. Unlike the probabilistic association methods, the proposed soft localization algorithm uses a consistency metric to find the LoS paths. For data association, the following cost function is used to find the LoS paths [36]:

$$\rho = \begin{cases} 1, & (\hat{\mathbf{x}}_{a} - \hat{\mathbf{x}}_{b})^{T} (\hat{\mathbf{V}}_{a} + \hat{\mathbf{V}}_{b})^{-1} (\hat{\mathbf{x}}_{a} - \hat{\mathbf{x}}_{b}) < \zeta^{2}, \\ 0, & \text{otherwise}, \end{cases}$$
(50)

where  $\rho$  is the data fusion indicator and  $\zeta$  is a tunable parameter. If  $\rho = 1$ , the data fusion of  $f_N(\hat{\mathbf{x}}_a, \hat{\mathbf{V}}_a)$  and  $f_N(\hat{\mathbf{x}}_b, \hat{\mathbf{V}}_b)$  is performed using (49). For  $f_N(\hat{\mathbf{x}}_u, \hat{\mathbf{V}}_u)$ , according to the pdf of Gaussian distribution, the elliptical region

$$(\mathbf{x} - \hat{\mathbf{x}}_{\mathbf{u}})\hat{\mathbf{V}}_{\mathbf{u}}^{-1}(\mathbf{x} - \hat{\mathbf{x}}_{\mathbf{u}}) = \zeta^{2}$$
 (51)

corresponds to the probability  $\operatorname{erf}(\zeta/\sqrt{2})$ , where  $\mathbf{x}=(x,y)^T$  and  $\operatorname{erf}(\cdot)$  is the Gaussian error function. The elliptical region contains 99.73% probability when  $\zeta=3$ . (50) implies that  $f_{\mathrm{N}}(\hat{\mathbf{x}}_{\mathrm{a}},\hat{\mathbf{V}}_{\mathrm{a}})$  and  $f_{\mathrm{N}}(\hat{\mathbf{x}}_{\mathrm{b}},\hat{\mathbf{V}}_{\mathrm{b}})$  are fused when the distance between the centers of two ellipses are smaller than a threshold characterized by  $\zeta$ .

Assume that the soft parameter estimates of receiver i are obtained as  $\hat{\mathbf{s}}_k^i$  and  $\hat{\mathbf{V}}_k^i$  with  $k=1,2,\cdots,L_i$ , where  $\hat{\mathbf{s}}_k^i$  and  $\hat{\mathbf{V}}_k^i$  are defined as

$$\hat{\mathbf{s}}_k^i = \left(\hat{\theta}_k^i, \hat{\eta}_k^i\right)^T, \tag{52}$$

$$\hat{\mathbf{V}}_{k}^{i} = \begin{bmatrix} \hat{v}_{\theta\theta,k}^{i} & \hat{v}_{\theta\eta,k}^{i} \\ \hat{v}_{\theta\eta,k}^{i} & \hat{v}_{\eta\eta,k}^{i} \end{bmatrix}. \tag{53}$$

In addition, there are R receivers. In the following analysis, standard and light versions of the soft localization algorithm are proposed for the perfect synchronization case on the basis of the EP-SLAM algorithm framework.

1) Standard Version: The procedures of the standard version are summarized as follows.

**Initialization**: Parameter  $\zeta$  of cost function.

**Input**:  $\hat{\mathbf{s}}_k^i$  and  $\hat{\mathbf{V}}_k^i$  with  $k=1,2,\cdots,L_i$  and  $i=1,2,\cdots,R$ .

**Step 1) User position inference**: Given  $\hat{\mathbf{s}}_k^i$  and  $\hat{\mathbf{V}}_k^i$ , the soft user position  $f_{\mathrm{N}}(\hat{\mathbf{x}}_{\mathrm{u},k}^i, \hat{\mathbf{V}}_{\mathrm{u},k}^i)$  can be inferred at receiver i with  $\mathbf{x}_{\mathrm{b}}^i$  and  $\omega_i$  by using the results of Section IV-A. Receiver i obtains  $L_i$  soft user positions.

### Step 2) User position association and fusion:

- a) A receiver combination with R soft user positions can be obtained by selecting a soft user position from each receiver. Overall, there are  $\prod_{i=1}^{R} L_i$  receiver combinations.
- b) For any receiver combination, there are  $C_R^1 + C_R^2 + \cdots + C_R^R = 2^R 1$  combinations for R soft user positions. At least one of the  $(2^R 1) \prod_{i=1}^R L_i$  combinations

contains all the soft user positions generated by the LoS path.

- c) For any combination with more than one soft user position, the data association and fusion are sequentially performed. For example, suppose a combination contains the  $f_N(\hat{\mathbf{x}}_{u,1}, \mathbf{V}_{u,1}), f_N(\hat{\mathbf{x}}_{u,2}, \mathbf{V}_{u,2}),$ and  $f_{\rm N}(\hat{\mathbf{x}}_{{\rm u},3},\hat{\mathbf{V}}_{{\rm u},3}).$  First, if the cost function of  $f_{\rm N}(\hat{\mathbf{x}}_{{\rm u},1},\hat{\mathbf{V}}_{{\rm u},1})$  and  $f_{\rm N}(\hat{\mathbf{x}}_{{\rm u},2},\hat{\mathbf{V}}_{{\rm u},2})$  implies  $\rho=1$ , then  $f_N(\hat{\mathbf{x}}_{\mathrm{u},12},\hat{\mathbf{V}}_{\mathrm{u},12})$  can be obtained by fusing  $f_{\rm N}(\hat{\mathbf{x}}_{\rm u,1},\hat{\mathbf{V}}_{\rm u,1})$  and  $f_{\rm N}(\hat{\mathbf{x}}_{\rm u,2},\hat{\mathbf{V}}_{\rm u,2})$ . Second, if the cost function of  $f_N(\hat{\mathbf{x}}_{u,12}, \hat{\mathbf{V}}_{u,12})$  and  $f_N(\hat{\mathbf{x}}_{u,3}, \hat{\mathbf{V}}_{u,3})$  implies  $\rho = 1$ , then  $f_N(\hat{\mathbf{x}}_{u,*}, \hat{\mathbf{V}}_{u,*})$  can be obtained using (49) analogously. If all the soft user positions of a combination can be fused together, then the final fusion result  $f_N(\hat{\mathbf{x}}_{u,*}, \mathbf{V}_{u,*})$  is saved; otherwise, this combination is discarded. For combinations with only a single soft user position  $f_N(\hat{\mathbf{x}}_u, \hat{\mathbf{V}}_u)$ , we have  $f_N(\hat{\mathbf{x}}_{u,*}, \hat{\mathbf{V}}_{u,*}) \leftarrow$  $f_{\rm N}(\hat{\mathbf{x}}_{\rm u}, \hat{\mathbf{V}}_{\rm u}).$
- d) For  $(2^R 1) \prod_{i=1}^R L_i$  combinations, the soft user position  $f_N(\hat{\mathbf{x}}_{u,*}, \hat{\mathbf{V}}_{u,*})$  with the least cost  $\operatorname{tr}(\hat{\mathbf{V}}_{u,*})$  is labeled as the user position estimate.

**Output**: User position estimate  $\hat{\mathbf{x}}_{u} = \hat{\mathbf{x}}_{u,*}$ .

Remark 2: The cost function measures the consistency of two soft user positions. If the distance between two soft user positions is lower than a threshold, then these two soft user positions are identified as two observations of a single source. The user position is the source that generates many LoS paths. The EP-SLAM algorithm framework solves the data association and fusion problems and obtains the user position estimate by finding the combination with the least cost (highest consistency)  $\operatorname{tr}(\hat{\mathbf{V}}_{\mathrm{u},*})$ .

2) Light Version: Because all the combinations are computed in the standard version, the computational complexity is extremely high when R and  $L_i$ ,  $i=1,2,\cdots,R$  are large. In the light version, only a single combination is considered. The procedures of the light version are summarized as follows:

**Initialization**: Parameter  $\zeta$  of cost function.

**Input**:  $\hat{\mathbf{s}}_k^i$  and  $\hat{\mathbf{V}}_k^i$  with  $k=1,2,\cdots,L_i$  and  $i=1,2,\cdots,R$ .

**Step 1) User position inference**: Given  $\hat{\mathbf{s}}_k^i$  and  $\hat{\mathbf{V}}_k^i$ , the soft user position  $f_{\mathrm{N}}(\hat{\mathbf{x}}_{\mathrm{u},k}^i, \hat{\mathbf{V}}_{\mathrm{u},k}^i)$  can be inferred at receiver i with  $\mathbf{x}_{\mathrm{b}}^i$  and  $\omega_i$  by using the results of Section IV-A. Receiver i obtains  $L_i$  soft user positions.

# Step 2) User position association and fusion:

- a) According to the analysis of [36], the soft user position generated by the LoS path generally has the least cost. Therefore, for receiver i, the soft user position estimate with the least cost  $\operatorname{tr}(\hat{\mathbf{V}}_{\mathrm{u}})$  is selected from  $L_i$  soft user position estimates. The R soft user position estimates from the R receivers are reindexed as  $f_{\mathrm{N}}(\hat{\mathbf{x}}_{\mathrm{u},i},\hat{\mathbf{V}}_{\mathrm{u},i}), i=1,2,\cdots,R$  in descending order of cost:  $\operatorname{tr}(\hat{\mathbf{V}}_{\mathrm{u},1}) < \operatorname{tr}(\hat{\mathbf{V}}_{\mathrm{u},2}) < \cdots < \operatorname{tr}(\hat{\mathbf{V}}_{\mathrm{u},R})$ .
- b) The data association and fusion are sequentially performed for  $f_{\rm N}(\hat{\mathbf{x}}_{{\rm u},i},\hat{\mathbf{V}}_{{\rm u},i}), i=1,2,\cdots,R$ . For example, suppose the combination contains  $f_{\rm N}(\hat{\mathbf{x}}_{{\rm u},1},\hat{\mathbf{V}}_{{\rm u},1}), f_{\rm N}(\hat{\mathbf{x}}_{{\rm u},2},\hat{\mathbf{V}}_{{\rm u},2})$ , and  $f_{\rm N}(\hat{\mathbf{x}}_{{\rm u},3},\hat{\mathbf{V}}_{{\rm u},3})$ . If the cost function

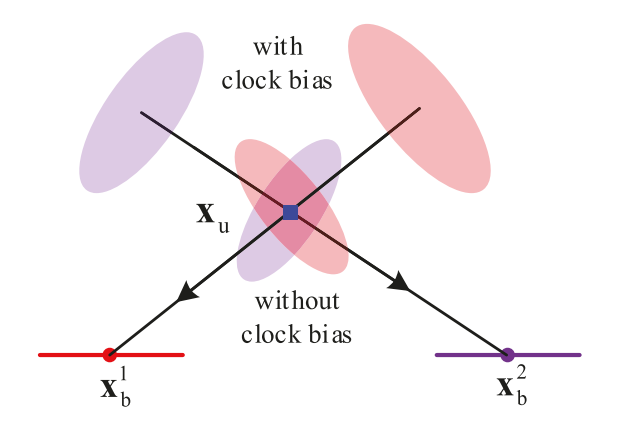


Fig. 2. Illustrations of soft user positions without and with clock bias.

of  $f_N(\hat{\mathbf{x}}_{\mathrm{u},1},\hat{\mathbf{V}}_{\mathrm{u},1})$  and  $f_N(\hat{\mathbf{x}}_{\mathrm{u},2},\hat{\mathbf{V}}_{\mathrm{u},2})$  implies  $\rho=0$ , then  $f_N(\hat{\mathbf{x}}_{\mathrm{u},2},\hat{\mathbf{V}}_{\mathrm{u},2})$  is discarded. If the cost function of  $f_N(\hat{\mathbf{x}}_{\mathrm{u},1},\hat{\mathbf{V}}_{\mathrm{u},1})$  and  $f_N(\hat{\mathbf{x}}_{\mathrm{u},3},\hat{\mathbf{V}}_{\mathrm{u},3})$  implies  $\rho=1$ , then  $f_N(\hat{\mathbf{x}}_{\mathrm{u},*},\hat{\mathbf{V}}_{\mathrm{u},*})$  can be obtained using (49). If the cost function of  $f_N(\hat{\mathbf{x}}_{\mathrm{u},1},\hat{\mathbf{V}}_{\mathrm{u},1})$  and any other soft user positions implies  $\rho=0$ , then we have  $f_N(\hat{\mathbf{x}}_{\mathrm{u},*},\hat{\mathbf{V}}_{\mathrm{u},*}) \leftarrow f_N(\hat{\mathbf{x}}_{\mathrm{u},1},\hat{\mathbf{V}}_{\mathrm{u},1})$ .

**Output**: User position estimate  $\hat{\mathbf{x}}_{u} = \hat{\mathbf{x}}_{u,*}$ .

#### C. Imperfect Synchronization Case

For the imperfect synchronization case, the clock bias  $\tau_{\rm u}$  and user position  $\mathbf{x}_{\rm u}$  need to be simultaneously estimated. Assume that we have two soft user positions  $f_{\rm N}(\hat{\mathbf{x}}_{\rm u,1},\hat{\mathbf{V}}_{\rm u,1})$  and  $f_{\rm N}(\hat{\mathbf{x}}_{\rm u,2},\hat{\mathbf{V}}_{\rm u,2})$  characterized by soft parameters  $\hat{\mathbf{s}}_1=(\hat{\theta}_1,\hat{\eta}_1)^T$  and  $\hat{\mathbf{V}}_1$  and  $\hat{\mathbf{s}}_2=(\hat{\theta}_2,\hat{\eta}_2)^T$  and  $\hat{\mathbf{V}}_2$  from two receivers with  $(\mathbf{x}_{\rm b}^1,\omega_1)$  and  $(\mathbf{x}_{\rm b}^2,\omega_2)$ , respectively. Fig. 2 shows examples of soft user positions  $f_{\rm N}(\hat{\mathbf{x}}_{\rm u,1},\hat{\mathbf{V}}_{\rm u,1})$  and  $f_{\rm N}(\hat{\mathbf{x}}_{\rm u,2},\hat{\mathbf{V}}_{\rm u,2})$  with and without clock bias  $\tau_{\rm u}$ . The soft user positions resemble ellipses. As shown in Fig. 2, without the clock bias  $\tau_{\rm u}$ ,  $f_{\rm N}(\hat{\mathbf{x}}_{\rm u,1},\hat{\mathbf{V}}_{\rm u,1})$  and  $f_{\rm N}(\hat{\mathbf{x}}_{\rm u,2},\hat{\mathbf{V}}_{\rm u,2})$  overlap and satisfy the cost function (50). With the clock bias  $\tau_{\rm u}$ ,  $f_{\rm N}(\hat{\mathbf{x}}_{\rm u,1},\hat{\mathbf{V}}_{\rm u,1})$  and  $f_{\rm N}(\hat{\mathbf{x}}_{\rm u,2},\hat{\mathbf{V}}_{\rm u,2})$  move away from each other, and they no longer satisfy the cost function (50) when  $\tau_{\rm u}$  is large enough.

At this point, we show how to estimate the clock bias  $\tau_{\rm u}$  for  $f_{\rm N}(\hat{\mathbf{x}}_{{\rm u},1},\hat{\mathbf{V}}_{{\rm u},1})$  and  $f_{\rm N}(\hat{\mathbf{x}}_{{\rm u},2},\hat{\mathbf{V}}_{{\rm u},2})$ . According to (41), the distance between  $\hat{\mathbf{x}}_{{\rm u},1}$  and  $\hat{\mathbf{x}}_{{\rm u},2}$  can be written as

$$d^{2} = (x_{b}^{1} - x_{b}^{2} + \mu_{p1}(\hat{\eta}_{1} - \eta_{u}) - \mu_{p2}(\hat{\eta}_{2} - \eta_{u}))^{2} + (y_{b}^{1} - y_{b}^{2} + \mu_{q1}(\hat{\eta}_{1} - \eta_{u}) - \mu_{q2}(\hat{\eta}_{2} - \eta_{u}))^{2}, \quad (54)$$

where

$$\mu_{p1} = \frac{c}{2\pi f_{\rm D}} \cos(\hat{\theta}_1 + \omega_1), \tag{55a}$$

$$\mu_{p2} = \frac{c}{2\pi f_{\rm D}} \cos(\hat{\theta}_2 + \omega_2),\tag{55b}$$

$$\mu_{q1} = \frac{c}{2\pi f_{\mathcal{D}}} \sin(\hat{\theta}_1 + \omega_1), \tag{55c}$$

$$\mu_{q2} = \frac{c}{2\pi f_{\rm D}} \sin(\hat{\theta}_2 + \omega_2). \tag{55d}$$

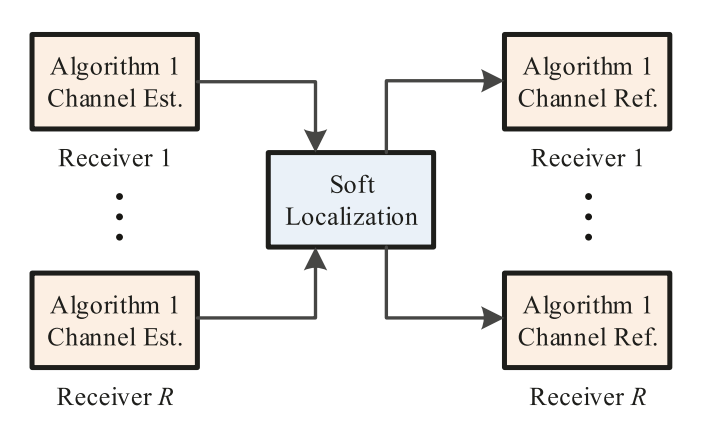


Fig. 3. Illustration of integrated communication and localization system.

For the perfect synchronization case,  $\eta_u = 0$ . Using some algebraic operations, the global minimum of  $d^2$  is achieved at

$$\hat{\eta}_{u} = \frac{c_{1}(\mu_{p1} - \mu_{p2}) + c_{2}(\mu_{q1} - \mu_{q2})}{(\mu_{p1} - \mu_{p2})^{2} + (\mu_{q1} - \mu_{q2})^{2}},$$
(56)

where

$$c_1 = x_b^1 - x_b^2 + \mu_{p1}\hat{\eta}_1 - \mu_{p2}\hat{\eta}_2,$$
 (57a)

$$c_2 = y_b^1 - y_b^2 + \mu_{q1}\hat{\eta}_1 - \mu_{q2}\hat{\eta}_2.$$
 (57b)

We then have the updates  $\hat{\eta}_1 \leftarrow \hat{\eta}_1 - \hat{\eta}_u$  and  $\hat{\eta}_2 \leftarrow \hat{\eta}_2 - \hat{\eta}_u$ . If the updated  $\hat{\eta}_1$  and  $\hat{\eta}_2$  satisfy  $0 < \hat{\eta}_1 < 2\pi$  and  $0 < \hat{\eta}_2 < 2\pi$ , then  $f_N(\hat{\mathbf{x}}_{u,1}, \hat{\mathbf{V}}_{u,1})$  and  $f_N(\hat{\mathbf{x}}_{u,2}, \hat{\mathbf{V}}_{u,2})$  can be recomputed using  $(\hat{\mathbf{s}}_1, \hat{\mathbf{V}}_1)$  and  $(\hat{\mathbf{s}}_2, \hat{\mathbf{V}}_2)$ , respectively, according to the approach proposed in Section IV-A. If the updated  $f_N(\hat{\mathbf{x}}_{u,1}, \hat{\mathbf{V}}_{u,1})$  and  $f_N(\hat{\mathbf{x}}_{u,2}, \hat{\mathbf{V}}_{u,2})$  satisfy the cost function (50), then  $\hat{\tau}_u = \hat{\eta}_u/(2\pi f_D)$  is a possible clock bias estimate.

According to the analysis, the light version of the soft localization algorithm is proposed as follows:

**Initialization**: Parameter  $\zeta$  of cost function.

**Input**:  $\hat{\mathbf{s}}_k^i$  and  $\hat{\mathbf{V}}_k^i$  with  $k=1,2,\cdots,L_i$  and  $i=1,2,\cdots,R$ .

Step 1) User position inference: Given  $\hat{\mathbf{s}}_k^i$  and  $\hat{\mathbf{V}}_k^i$ , the soft user position  $f_{\mathrm{N}}(\hat{\mathbf{x}}_{\mathrm{u},k}^i,\hat{\mathbf{V}}_{\mathrm{u},k}^i)$  can be inferred at receiver i with  $\mathbf{x}_{\mathrm{b}}^i$  and  $\omega_i$  by using the results of Section IV-A. Receiver i obtains  $L_i$  soft user positions.

# **Step 2) User position association and fusion:**

- a) For receiver i, the soft user position estimate with the least cost  $\operatorname{tr}(\hat{\mathbf{V}}_{\mathbf{u}})$  is selected from  $L_i$  soft user position estimates. The R soft user position estimates from R receivers are reindexed as  $f_{\mathbf{N}}(\hat{\mathbf{x}}_{\mathbf{u},i},\hat{\mathbf{V}}_{\mathbf{u},i}), i=1,2,\cdots,R$  in descending order of cost:  $\operatorname{tr}(\hat{\mathbf{V}}_{\mathbf{u},1}) < \operatorname{tr}(\hat{\mathbf{V}}_{\mathbf{u},2}) < \cdots < \operatorname{tr}(\hat{\mathbf{V}}_{\mathbf{u},R})$ .
- b) For any two soft user positions, the clock bias  $\hat{\tau}_{\rm u} = \hat{\eta}_{\rm u}/(2\pi f_{\rm D})$  can be estimated using (56).
- c) For the clock bias  $\hat{\tau}_{\rm u} = \hat{\eta}_{\rm u}/(2\pi f_{\rm D})$ , the soft user positions  $f_{\rm N}(\hat{\mathbf{x}}_{{\rm u},i},\hat{\mathbf{V}}_{{\rm u},i}), i=1,2,\cdots,R$  are recomputed with  $\eta\leftarrow\eta-\hat{\eta}_{\rm u}$ . The data association and fusion are sequentially performed for  $f_{\rm N}(\hat{\mathbf{x}}_{{\rm u},i},\hat{\mathbf{V}}_{{\rm u},i}), i=1,2,\cdots,R,$  and the final fusion result is given by  $f_{\rm N}(\hat{\mathbf{x}}_{{\rm u},*},\hat{\mathbf{V}}_{{\rm u},*})$ .

d) For all the possible clock bias estimates, the soft user position  $f_N(\hat{\mathbf{x}}_{\mathrm{u},*},\hat{\mathbf{V}}_{\mathrm{u},*})$  with the least cost  $\mathrm{tr}(\hat{\mathbf{V}}_{\mathrm{u},*})$  is labeled as the user position estimate.

**Output**: User position estimate  $\hat{\mathbf{x}}_{\mathrm{u}} = \hat{\mathbf{x}}_{\mathrm{u},*}$  and clock bias  $\hat{\tau}_{\mathrm{u}} = \hat{\eta}_{\mathrm{u}}/(2\pi f_{\mathrm{D}})$ .

The user position estimate  $\hat{\mathbf{x}}_u$  and clock bias  $\hat{\tau}_u$  can be further refined by minimizing the sum of the distances between  $\hat{\mathbf{x}}_u$  and each component  $\hat{\mathbf{x}}_{u,i}$  that were used to obtain  $\hat{\mathbf{x}}_u$ .

# D. Integrated Communication and Localization

The integrated communication and localization system is shown in Fig. 3. First, Algorithm 1 is implemented at each receiver in parallel to solve the channel estimation problem and obtain the soft parameter estimates. Second, the soft parameter estimates of all the receivers are transmitted to the data center to implement the soft localization algorithm. Finally, the propagation parameters  $\hat{\theta}_i^0$  and  $\hat{\tau}_i^0$  can be obtained using the user position estimate  $\hat{\mathbf{x}}_{\mathbf{u}}$  and the topology condition (5) for receiver i. Given fixed  $\hat{\theta}_i^0$  and  $\hat{\tau}_i^0$ , the channel estimate of receiver i can be refined through the Newton gradient descent updates of Algorithm 1 if receiver i has the LoS path.

Remark 3: Designing a turbo-based approach to combine the soft channel estimation and localization algorithms is possible because the algorithms produce soft estimates. However, additional turbo iterations between the two algorithms cannot provide additional performance improvement. The same is not true for turbo detection in MIMO systems, where the transmitted symbols are chosen from several discrete constellations and information regarding the symbols is known. Therefore, a performance improvement from a turbo-based algorithm is expected in MIMO detection. By contrast, the topology condition (5) only imposes a consistency constraint between the different LoS paths by forcing them to come from a single source at the user position. Finding a single source implies a good user position estimate, but such an estimate does not provide true prior information of the user position. Hence, additional iterations do not provide further improvement.

#### V. NUMERICAL RESULTS

The performance of the proposed algorithms are verified in this section by computer simulations. First, an outdoor mmWave system is investigated, as shown in Fig. 4. The system has 16 receivers, which are deployed around the sides of a rectangular region; the user is located at (35,28). The ULA rotation  $\omega_i$  of receivers 1 to 16 are given by  $0^\circ, 0^\circ, 0^\circ, 0^\circ, 180^\circ, 180^\circ, 180^\circ, 180^\circ, -90^\circ, -90^\circ, -90^\circ, -90^\circ, 90^\circ, 90^\circ, 90^\circ, and 90^\circ. For the imperfect synchronization case, the clock bias is <math display="inline">\tau_{\rm u}=1$  ms. Each receiver has M=8 antennas and uses N=128 subcarriers with spacing  $f_\triangle=60$  kHz, and the bandwidth of the system is 7.68 MHz. The system operates at 28 GHz, which means that the carrier wavelength is  $\lambda=1.07$  cm, and the power spectral density of the AWGN at the receiver side is -164 dBm/Hz. A free space path loss model is assumed for the LoS path as follows:

$$\beta_{\rm los}^i = \sqrt{\frac{G_t G_r \lambda^2}{16\pi^2 d_i^2}},\tag{58}$$

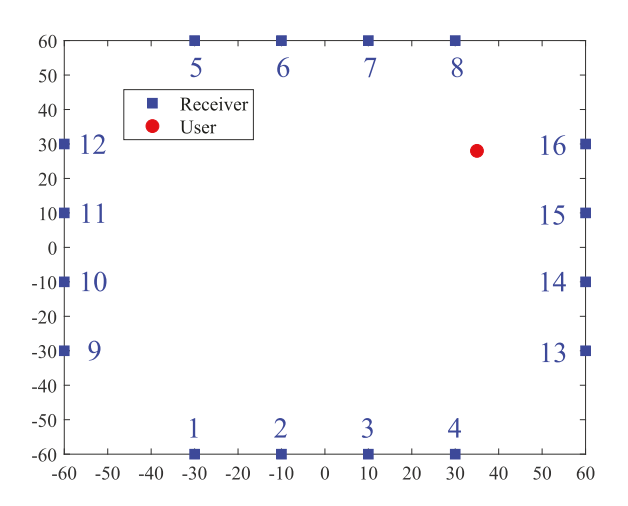


Fig. 4. Illustration of outdoor mmWave system assumed in the simulations.

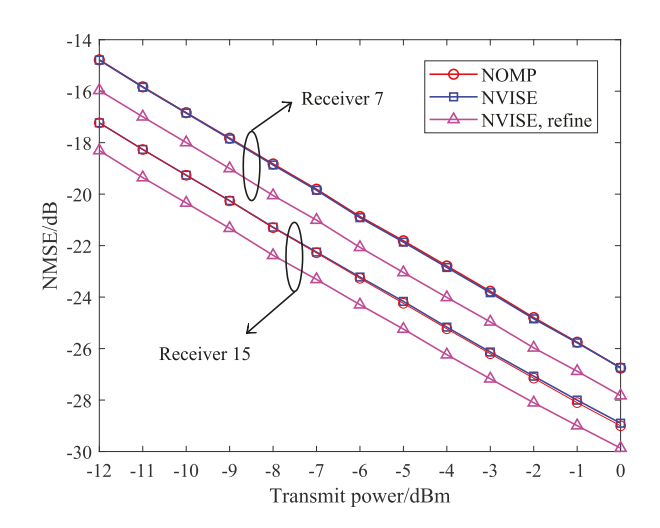


Fig. 5. NMSE of channel estimate for receivers 7 and 15.

TABLE I
RECEIVED SNR OF THE LOS PATH FOR EACH RECEIVER

Receiver	1	2	3	4	5	6	7	8
SNR/dB	-7.0	-6.1	-5.5	-5.1	-3.4	-1.0	1.6	3.6
Receiver	9	10	11	12	13	14	15	16
SNR/dB	-7.2	-6.4	-5.9	-5.8	-2.2	0.6	4.0	5.8

where  $G_t = G_r = 1$  and  $d_i$  is the distance between the user and receiver i. Each receiver has an NLoS path, whose power is one-third that of the LoS path. The angle and delay of the NLoS path are randomly generated.

Fig. 4 shows that many of the receivers are far from the user, and thus, their received signal power is weak. Table I shows the received signal-to-noise ratio (SNR) of the LoS path at each receiver when the transmit power is 0 dBm. This table indicates that the user is visible to only a small fraction of the receivers. If a coarse user position estimate is available, which can be obtained by user tracking, then a specific subset of the receivers can be used to serve this user for channel estimation, data transmission, localization, and position-based communication services. In addition, the mmWave system can serve multiple spatially distant users with the same time frequency resources.

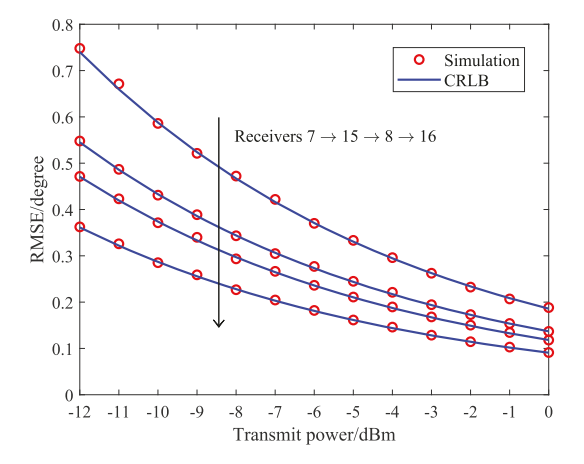


Fig. 6. RMSE of AoA estimate  $\hat{\theta}$  (LoS path) for receivers 7, 8, 15, and 16.

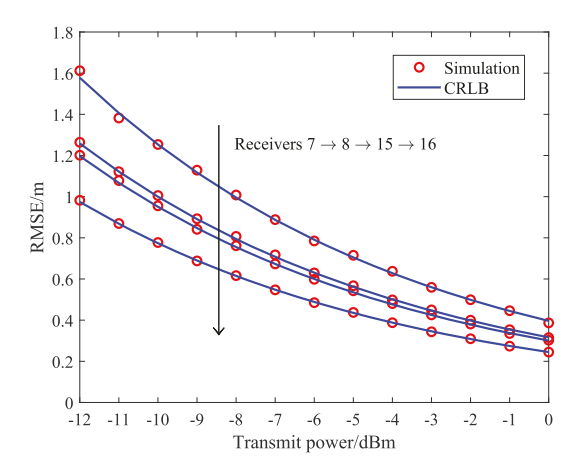


Fig. 7. RMSE of distance estimate  $c\hat{\tau}$  (LoS path) for receivers 7, 8, 15, and 16, where c is the speed of light.

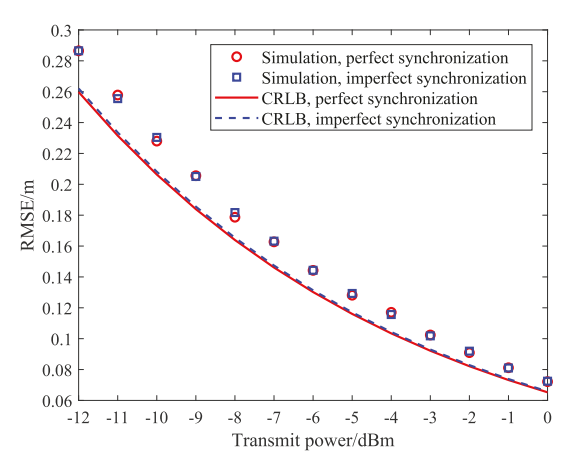


Fig. 8. RMSE of soft localization algorithm.

Sections V-A and V-B assume that only receivers 7, 8, 15, and 16 receive an LoS path from the user.

## A. Channel Estimation Performance

The NVISE algorithm uses a  $10\times$  oversampling rate, which means  $\gamma_M=\gamma_N=10$ . In addition,  $R_s=R_c=5$  and L=2.

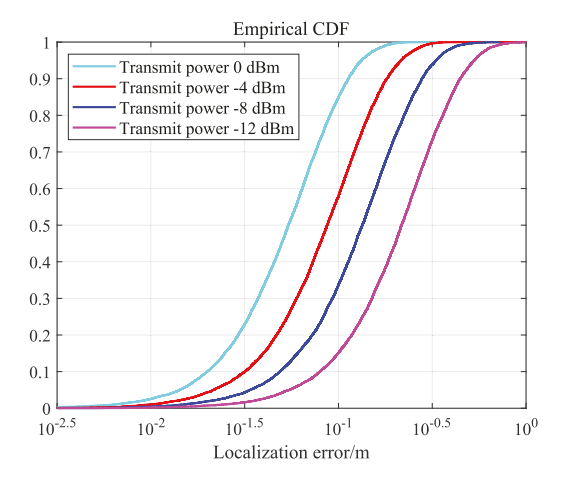


Fig. 9. Empirical cdf of localization error for different transmit power levels.

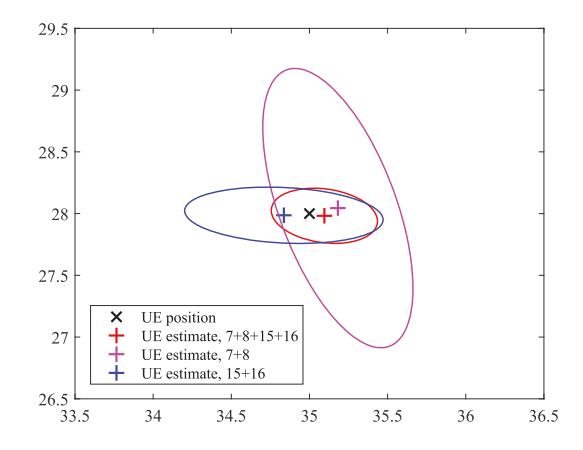
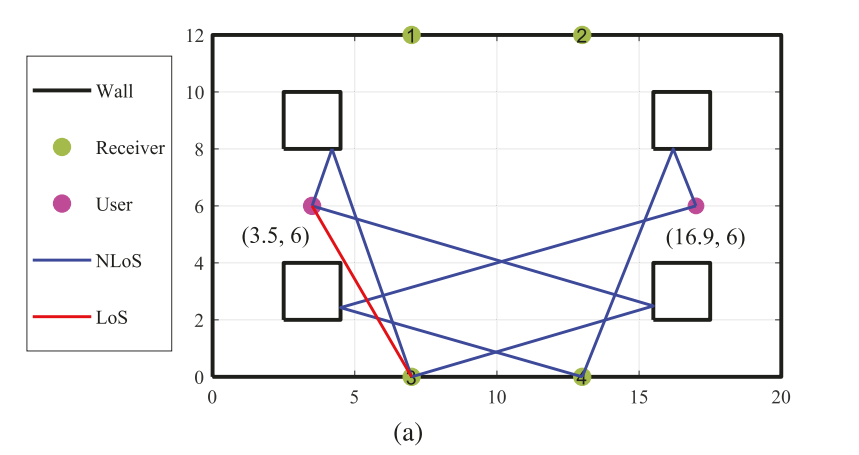


Fig. 10. Spatial distribution of soft localization output.

Fig. 5 shows the normalized mean squared error (NMSE) of the channel estimate for receivers 7 and 15. Receiver 15 shows a better performance than receiver 7 because it is near the user. For comparison, the channel estimation performance of the NOMP algorithm [16] is considered. The NOMP algorithm uses gridless Newton refinement to remove the grid effect of the OMP algorithm, and its performance can approach that of the CRLB. For the NOMP algorithm, the oversampling rates are  $\gamma_M = \gamma_N = 10$ , and the number of single and cyclic Newton refinements are both equal to 5. In addition, NOMP extracts L=2paths in each experiment. As shown in Fig. 5, the performance of the NVISE algorithm is similar to that of the NOMP algorithm. NVISE and NOMP use the same grid detection (30) for initialization, and the computational complexity of grid detection is  $\mathcal{O}(MN\log(MN))$ . In addition, NVISE and NOMP use the same Newton gradient descent approach, and the computational complexity of each Newton gradient descent is  $\mathcal{O}(MN)$ . Thus, the computation complexity of NVISE is comparable to that of NOMP.

Fig. 6 depicts the root mean square error (RMSE) of the AoA estimate of the LoS path for receivers 7, 8, 15, and 16, with the NVISE algorithm performed at each receiver independently. In addition, the CRLB is derived for each receiver independently. Appendix A shows the derivation details. The AoA estimate



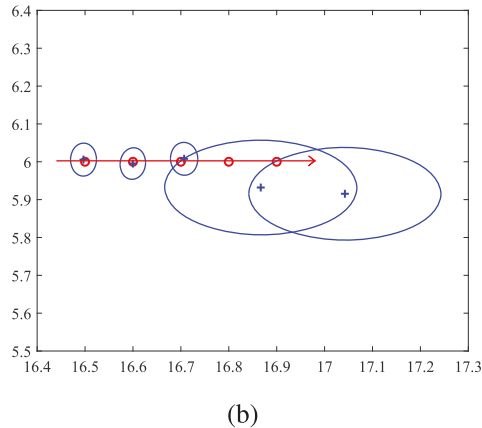


Fig. 11. (a) Illustration of the indoor mmWave scenario. (b) User position estimates and the corresponding elliptical regions for different user positions. The red dot shows the actual user position, while the blue "+" denotes the user position estimate, and the blue ellipse shows the region with 99.73% confidence level ( $\zeta = 3$ ). There is a sudden increase in the elliptical region when two of the LoS paths are blocked.

of the NVISE algorithm approaches that of the CRLB at every SNR level. Similar conclusions are obtained for the delay as shown in Fig. 7. According to Table I, the received SNRs of the receivers satisfy 7 < 8 < 15 < 16. Therefore, the delay estimate performance of receiver 8 is worse than that of receiver 15. However, for AoA  $\theta$ , the resolution increases when  $\theta$  moves toward  $90^{\circ}$  for the ULA array. Consequently, unlike the case of the delay estimate, the AoA estimate performance of receiver 8 is better than that of receiver 15 because the AoA of receiver 8 is  $98.9^{\circ}$  while that of receiver 15 is  $54.2^{\circ}$ .

Imposing the geometrical constraint of the LoS paths of receivers in soft localization can improve the AoA and delay estimate performance. In Section IV-D, the AoA and delay estimates of the LoS path for each receiver are recomputed using user position after the soft localization. Then, the AoA and delay estimates of the NLoS paths are recomputed through the Newton method with a fixed LoS path. The channel estimation performance is further improved because the AoA and delay estimates of the LoS path are refined. As shown in Fig. 5, the refinement provides a gain of nearly 1 dB.

### B. Localization Performance

In this section, we study the accuracy of the proposed soft localization algorithms. Fig. 8 depicts the RMSE localization performance of the light version of the soft localization algorithms for perfect and imperfect synchronization cases with  $\zeta = 3$ . The results show that the soft localization algorithms can provide decimeter-level localization accuracy. The CRLB considers the relationship between the user position and the AoAs and delays at the receivers. Appendix A shows further details. The performance of the perfect and imperfect synchronization cases approach their CRLBs, respectively. In addition, the performance of the imperfect synchronization case is nearly the same as that of the perfect synchronization case, thus verifying the effectiveness of the soft localization algorithms. Fig. 9 plots the empirical cumulative distribution function (cdf) of the localization error for the perfect synchronization case, where the localization error is given by  $\sqrt{(\mathbf{x}_{\mathrm{u}} - \mathbf{x})^T(\mathbf{x}_{\mathrm{u}} - \mathbf{x})}$ . The performance improves uniformly with the transmit power, showing a 84.9% success rate in achieving an accuracy of better than 10 cm when the transmit power is 0 dBm.

Herein, we use an example to show how soft localization works. Fig. 10 depicts the elliptical regions with  $\zeta = 3$  of a random realization for the perfect synchronization case, where the transmit power is -6 dBm. Receivers 7, 8, 15, and 16 in case I are assumed to have LoS paths while only receivers 7 and 8 have LoS paths in case II, and only receivers 15 and 16 have LoS paths in case III. The localization errors for cases II and III are 18.7 and 16.4 cm, respectively. The elliptical region of case II is larger than that of case III because receivers 7 and 8 have smaller received SNRs than receivers 15 and 16. Case I shows the best performance (9.7 cm localization error) and the smallest elliptical region because of the two additional receivers. The proposed soft localization algorithms are scalable for localization. For example, as the user position is static in Fig. 4, the user position estimate can be easily refined by incorporating extra soft information into the Gaussian distribution using the Gaussian reproduction formula.

The localization performance relies heavily on the propagation environment. Leveraging the proposed soft localization algorithms, the accuracy of the user position estimate can be easily evaluated through its spatial distribution. Such feature is useful in many position-based communication services, such as user position tracking. Next, we discuss the use of soft localization in a different indoor propagation environment. Fig. 11(a) shows the layout of an indoor room (20 m  $\times$  12 m) with four obstacles (pillars) distributed around the room. The system has four receivers deployed on the front and back walls of the room, and the ULA rotations of receivers 1 to 4 are given by 180°, 180°, 0°, and 0°. Ray tracing is used to compute the LoS and NLoS paths, as shown in Fig. 11(a). Only first-order reflections are considered because of the high attenuation in mmWave bands. The free space path loss model of (58) is adopted, and the reflection via the wall is assumed to cause an additional 3 dB loss. The transmit power of the user is -10 dBm, and the other system settings remain the same as those in Sections V-A. Two different scenarios are considered. In case I, the user is located at (3.5,6), and Fig. 11(a) shows that all the receivers see an LoS path. A user located at (16.5,6) would have the same performance as one at (3.5,6) because the layout of the room is symmetrical. For case II, the user moves to the right from (16.5,6) to (16.9,6). The LoS paths for receivers 2 and 4 in case II are blocked by the pillars despite the fact that the user only moves 40 cm. Fig. 11(b) shows the elliptical regions with 99.73% confidence levels at different positions as the user moves from (16.5,6) to (16.9,6) in steps of 10 cm. We see that the size of the elliptical region suddenly increases when the user moves from (16.7,6) to (16.8,6) because it is at this point that the LoS paths of receivers 2 and 4 become blocked.

#### VI. CONCLUSION

Soft channel estimation and the soft localization algorithms are proposed in this study for perfect and imperfect synchronization cases. The proposed algorithms use a fully Bayesian approach to extract soft information of the AoAs and delays of user signals at several receivers, reconstructs the equivalent channel, and localizes the user position. The performance of the proposed algorithms are extensively studied. The results show that the proposed algorithms can approach the CRLB for channel estimation and localization. The impact of the propagation environment on localization performance is presented for a static case. Moreover, evolving confidence levels are plotted on the basis of the estimated soft position information for a moving user. These evaluations show that the algorithms have promise for a variety of position-based communication services, such as resource allocation, beam alignment, and interference control.

# APPENDIX A THE DERIVATION OF CRLB

The CRLBs of the AoA and delay (distance) are discussed first. For any receiver, the received signal can be written as

$$\mathbf{Y} = h_1 e^{j\phi_1} \mathbf{a}(\theta_1) \mathbf{b}^T(\eta_1) + h_2 e^{j\phi_2} \mathbf{a}(\theta_2) \mathbf{b}^T(\eta_2) + \mathbf{W}.$$
 (59)

In the RHS of (59), the first term represents the LoS path and the second term denotes the NLoS path. The frequency  $\eta_1$  can be expressed as

$$l_1 = c\tau_1 = \frac{c}{2\pi f_D} \eta_1, \tag{60}$$

where c is the speed of light and  $l_1$  is the length of LoS path. For the element in the m-th row and n-th column of  $\mathbf{Y}$ , the first-order derivatives are given by

$$v_{\theta_1}^{mn} = -j(m-1)\pi \sin(\theta_1)h_1 e^{j\phi_1} e^{j(m-1)\pi \cos(\theta_1)} e^{j(n-1)\eta_1},$$
(61a)

$$v_{l_1}^{mn} = j(n-1)\frac{2\pi f_{\rm D}}{c}h_1e^{j\phi_1}e^{j(m-1)\pi\cos(\theta_1)}e^{j(n-1)\eta_1},$$
 (61b)

$$v_{h_1}^{mn} = e^{j\phi_1} e^{j(m-1)\pi\cos(\theta_1)} e^{j(n-1)\eta_1}, \tag{61c}$$

$$v_{\phi_1}^{mn} = jh_1 e^{j\phi_1} e^{j(m-1)\pi\cos(\theta_1)} e^{j(n-1)\eta_1}.$$
 (61d)

In particular,  $\mathbf{v}_{\theta_1} \in \mathbb{C}^{MN \times 1}$  is the vector which contains  $v_{\theta_1}^{mn}, m = 1, 2, \cdots, M, n = 1, 2, \cdots, N$ . Similar definitions hold for  $\mathbf{v}_{l_1}$  with  $v_{l_1}^{mn}$ ,  $\mathbf{v}_{h_1}$  with  $v_{h_1}^{mn}$ , and  $\mathbf{v}_{\phi_1}$  with  $v_{\phi_1}^{mn}$ . Moreover, we have  $\mathbf{V} = (\mathbf{v}_{\theta_1}, \mathbf{v}_{l_1}, \mathbf{v}_{h_1}, \mathbf{v}_{\phi_1})$ . Therefore, the Fisher information matrix  $\mathbf{F}$  can be obtained as

$$\mathbf{F} = \frac{2}{v_w} \text{Re}(\mathbf{V}^H \mathbf{V}). \tag{62}$$

The CRLB is given by  $\mathbf{F}^{-1}$ . The elements with indicies (1,1) and (2,2) of  $\mathbf{F}^{-1}$  are the CRLBs for the AoA and delay (distance), respectively.

The CRLB of the user position is derived in the following analysis. According to (5), we have

$$\theta_1 = \operatorname{arccot}\left(\frac{(x_{\mathrm{u}} - x_{\mathrm{b}})\cos(\omega) + (y_{\mathrm{u}} - y_{\mathrm{b}})\sin(\omega)}{(y_{\mathrm{u}} - y_{\mathrm{b}})\cos(\omega) - (x_{\mathrm{u}} - x_{\mathrm{b}})\sin(\omega)}\right), \quad (63)$$

$$\eta_1 = \frac{2\pi f_{\rm D}}{c} \sqrt{(x_{\rm u} - x_{\rm b})^2 + (y_{\rm u} - y_{\rm b})^2},\tag{64}$$

where  $(x_{\rm u}, y_{\rm u})^T$  is the user position,  $(x_{\rm b}, y_{\rm b})^T$  and  $\omega$  are the position and ULA rotation of the receiver, respectively. For the element in the m-th row and n-th column of  $\mathbf{Y}$ , the first-order derivatives can be obtained as

$$v_{x_{u}} = h_{1}e^{j\phi_{1}}e^{j(m-1)\pi\cos(\theta_{1})}e^{j(n-1)\eta_{1}}$$

$$\times \left[j(m-1)\pi\sin(\theta_{1})\frac{y_{u} - y_{b}}{(x_{u} - x_{b})^{2} + (y_{u} - y_{b})^{2}}\right]$$

$$+ j(n-1)\frac{2\pi f_{D}}{c}\frac{x_{u} - x_{b}}{\sqrt{(x_{u} - x_{b})^{2} + (y_{u} - y_{b})^{2}}}\right],$$
(65a)

$$v_{y_{u}} = h_{1}e^{j\phi_{1}}e^{j(m-1)\pi\cos(\theta_{1})}e^{j(n-1)\eta_{1}}$$

$$\times \left[-j(m-1)\pi\sin(\theta_{1})\frac{x_{u}-x_{b}}{(x_{u}-x_{b})^{2}+(y_{u}-y_{b})^{2}}\right]$$

$$+ j(n-1)\frac{2\pi f_{D}}{c}\frac{y_{u}-y_{b}}{\sqrt{(x_{u}-x_{b})^{2}+(y_{u}-y_{b})^{2}}}\right].$$
(65b)

Moreover, we have  $\mathbf{V} = (\mathbf{v}_{x_u}, \mathbf{v}_{y_u}, \mathbf{v}_{h_1}, \mathbf{v}_{\phi_1})$ , and the definitions of  $\mathbf{v}_{x_u}$  and  $\mathbf{v}_{y_u}$  are similar to that of  $\mathbf{v}_{h_1}$  and  $\mathbf{v}_{\phi_1}$ . The Fisher information matrix  $\mathbf{F}$  can be obtained analogously like (62). The CRLB of the user position is given by  $\sqrt{a+b}$ , where a and b are the elements with indicies (1,1) and (2,2) of  $\mathbf{F}^{-1}$ . The above analysis is for single receiver. For the case of multiple receivers, the CRLB of the user position should include information from all receivers (7,8,15, and 16).

For imperfect synchronization case,  $\eta_1$  is defined as

$$\eta_1 = \frac{2\pi f_{\rm D}}{c} \sqrt{(x_{\rm u} - x_{\rm b})^2 + (y_{\rm u} - y_{\rm b})^2} + \eta_{\rm u}, \quad (66)$$

where  $\eta_{\rm u} = 2\pi f_{\rm D} \tau_{\rm u}$  and  $\tau_{\rm u}$  is the clock bias. For the element in the m-th row and n-th column of  $\mathbf{Y}$ , the first-order derivative with respect to  $\eta_{\rm u}$  is given by

$$v_{\eta_{\mathbf{u}}} = j(n-1)h_1 e^{j\phi_1} e^{j(m-1)\pi\cos(\theta_1)} e^{j(n-1)\eta_1}.$$
 (67)

 $\mathbf{V} = (\mathbf{v}_{x_{\mathrm{u}}}, \mathbf{v}_{y_{\mathrm{u}}}, \mathbf{v}_{\eta_{\mathrm{u}}}, \mathbf{v}_{h_{1}}, \mathbf{v}_{\phi_{1}})$  can be derived accordingly, where  $\mathbf{v}_{\eta_{\mathrm{u}}}$  follow the definition similar to  $\mathbf{v}_{h_{1}}$ . Analogously, we can obtain  $\mathbf{F}$  and the corresponding CRLB of localization for imperfect synchronization case with multiple receivers. According to (65b) and (67), for single receiver,  $\mathbf{F}$  is a singular matrix. This result coincides with the common sense, because the clock bias cannot be estimated with a single receiver.

#### REFERENCES

- F. Boccardi, R. W. Heath, A. Lozano, T. L. Marzetta, and P. Popovski, "Five disruptive technology directions for 5G," *IEEE Commun. Mag.*, vol. 52, no. 2, pp. 74–80, Feb. 2014.
- [2] T. S. Rappaport, R. W. Heath, R. C. Daniels, and J. N. Mutdock, *Millimeter Wave Wireless Communication*. Englewood Cliffs, NJ, USA: Prentice-Hall, 2014.
- [3] Z. Xiao and Y. Zeng, "An overview on integrated localization and communication towards 6G," Sci. China Inf. Sci., vol. 65, no. 3, pp. 1–46, Mar. 2022.
- [4] A. Yassin et al., "Recent advances in indoor localization: A survey on theoretical approaches and applications," *IEEE Commun. Surv. Tuts.*, vol. 19, no. 2, pp. 1327–1346, Apr.–Jun. 2017.
- [5] J. Yang, X. Yang, C.-K. Wen, and S. Jin, "Integrated sensing and communication with multi-domain cooperation," 2021, arXiv: 2105.03065.
- [6] E. C. Strinati et al., "Wireless environment as a service enabled by reconfigurable intelligent surfaces: The RISE-6G perspective," in *Proc. Eur. Conf. Netw. Commun.*, 2021, pp. 562–567.
- [7] J. He, H. Wymeersch, and M. Juntti, "Leveraging location information for RIS-aided mmWave MIMO communications," *IEEE Wireless Commun. Lett.*, vol. 10, no. 7, pp. 1380–1384, Jul. 2021.
- [8] A. Fascista, A. Coluccia, H. Wymeersch, and G. Seco-Granados, "RIS-aided joint localization and synchronization with a single-antenna mmwave receiver," in *Proc. IEEE Int. Conf. Acoust. Speech Signal Pro*cess., 2021, pp. 4455–4459.
- [9] M. Di Renzo et al., "Smart radio environments empowered by reconfigurable AI meta-surfaces: An idea whose time has come," EURASIP J. Wireless Commun. Netw., vol. 1, pp. 1–20, May 2019.
- [10] M. Di Renzo et al., "Smart radio environments empowered by reconfigurable intelligent surfaces: How it works, state of research, and the road ahead," *IEEE J. Sel. Areas Commun.*, vol. 38, no. 11, pp. 2450–2525, Nov. 2020
- [11] C. Huang et al., "Holographic MIMO surfaces for 6G wireless networks: Opportunities, challenges, and trends," *IEEE Wireless Commun.*, vol. 27, no. 5, pp. 118–125, Oct. 2020.
- [12] S. Rao, A. Mezghani, and A. L. Swindlehurst, "Channel estimation in one-bit massive MIMO systems: Angular versus unstructured models," *IEEE J. Sel. Top. Signal Process.*, vol. 13, no. 5, pp. 1017–1031, Sep. 2019.
- [13] D. Shutin and B. H. Fleury, "Sparse variational Bayesian SAGE algorithm with application to the estimation of multipath wireless channels," *IEEE Trans. Signal Process.*, vol. 59, no. 8, pp. 3609–3623, Aug. 2011.
- [14] C. Huang, L. Liu, C. Yuen, and S. Sun, "Iterative channel estimation using LSE and sparse message passing for mmWave MIMO systems," *IEEE Trans. Signal Process.*, vol. 67, no. 1, pp. 245–259, Jan. 2019.
- [15] C.-J. Wang, C.-K. Wen, S. Jin, and S.-H. Tsai, "Gridless channel estimation for mixed one-bit antenna array systems," *IEEE Trans. Wireless Commun.*, vol. 17, no. 12, pp. 8485–8501, Dec. 2018.
- [16] B. Mamandipoor, D. Ramasamy, and U. Madhow, "Newtonized orthogonal matching pursuit: Frequency estimation over the continuum," *IEEE Trans. Signal Process.*, vol. 64, no. 19, pp. 5066–5081, Oct. 2016.
- [17] M. Badiu, T. L. Hansen, and B. H. Fleury, "Variational Bayesian inference of line spectra," *IEEE Trans. Signal Process.*, vol. 65, no. 9, pp. 2247–2261, May 2017.
- [18] J. A. del Peral-Rosado, R. Raulefs, J. A. López-Salcedo, and G. Seco-Granados, "Survey of cellular mobile radio localization methods: From 1G to 5G," *IEEE Commun. Surv. Tuts.*, vol. 20, no. 2, pp. 1124–1148, May 2018.
- [19] F. Wen, H. Wymeersch, B. Peng, W. P. Tay, H. C. So, and D. Yang, "A survey on 5G massive MIMO localization," *Digit. Signal Process*, vol. 94, pp. 21–28, 2019, https://doi.org/10.1016/j.dsp.2019.05.005
- [20] N. Garcia, H. Wymeersch, E. G. Larsson, A. M. Haimovich, and M. Coulon, "Direct localization for massive MIMO," *IEEE Trans. Signal Process.*, vol. 65, no. 10, pp. 2475–2487, May 2017.

- [21] J. Yang, Y. Zeng, S. Jin, C.-K. Wen, and P. Xu, "Communication and localization with extremely large lens antenna array," *IEEE Trans. Wireless Commun.*, vol. 20, no. 5, pp. 3031–3048, May 2021.
- [22] Y. Wang and K. C. Ho, "An asymptotically efficient estimator in closed-form for 3-D AOA localization using a sensor network," *IEEE Trans. Wireless Commun.*, vol. 14, no. 12, pp. 6524–6535, Jul. 2015.
- [23] H. Wymeersch et al., "5G mmWave downlink vehicular positioning," in Proc. IEEE GLOBECOM, 2018, pp. 1–6.
- [24] K. C. Ho and W. W. Xu, "An accurate algebraic solution for moving source location using TDoA and FDoA measurements," *IEEE Trans. Signal Process.*, vol. 52, no. 9, pp. 2453–2463, Aug. 2004.
- [25] R. Amiri, F. Behnia, and H. Zamani, "Efficient 3-D positioning using timedelay and AoA measurements in MIMO radar systems," *IEEE Commun. Lett.*, vol. 21, no. 12, pp. 2614–2617, Aug. 2017.
- [26] J. Yang, S. Jin, C.-K. Wen, J. Guo, M. Matthaiou, and B. Gao, "Model-based learning network for 3-D localization in mmWave communications," *IEEE Trans. Wireless Commun.*, vol. 20, no. 8, pp. 5449–5466, Aug. 2021.
- [27] A. Conti, S. Mazuelas, S. Bartoletti, W. C. Lindsey, and M. Z. Win, "Soft information for localization-of-things," *Proc. IEEE*, vol. 107, no. 11, pp. 2240–2264, Nov. 2019.
- [28] S. Mazuelas, A. Conti, J. C. Allen, and M. Z. Win, "Soft range information for network localization," *IEEE Trans. Signal Process.*, vol. 66, no. 12, pp. 3155–3168, Jun. 2018.
- [29] Z. Yu, Z. Liu, F. Meyer, A. Conti, and M. Z. Win, "Localization based on channel impulse response estimates," in *Proc. IEEE/ION Position*, *Location Navigation Symp.*, 2020, pp. 1014–1021.
- [30] A. Venus, E. Leitinger, S. Tertinek, and K. Witrisal, "A message passing based adaptive PDA algorithm for robust radio-based localization and tracking," in *Proc. IEEE RadarConf.*, 2021, pp. 1–6.
- [31] E. Leitinger, F. Meyer, P. Meissner, K. Witrisal, and F. Hlawatsch, "Belief propagation based joint probabilistic data association for multipath-assisted indoor navigation and tracking," in *Proc. Int. Conf. Localization GNSS*, 2016, pp. 1–6.
- [32] E. Leitinger, F. Meyer, F. Tufvesson, and K. Witrisal, "Factor graph based simultaneous localization and mapping using multipath channel information," in *Proc. IEEE Int. Conf. Commun. Workshops*, 2017, pp. 652–658.
- [33] E. Leitinger, F. Meyer, F. Hlawatsch, K. Witrisal, F. Tufvesson, and M. Z. Win, "A belief propagation algorithm for multipath-based SLAM," *IEEE Trans. Wireless Commun.*, vol. 18, no. 12, pp. 5613–5629, Dec. 2019.
- [34] R. Mendrzik, F. Meyer, G. Bauch, and M. Z. Win, "Enabling situational awareness in millimeter wave massive MIMO systems," *IEEE J. Sel. Top. Signal Process.*, vol. 13, no. 5, pp. 1196–1211, Sep. 2019.
- [35] E. Leitinger, S. Grebien, and K. Witrisal, "Multipath-based SLAM exploiting AoA and amplitude information," in *Proc. IEEE Int. Conf. Commun. Workshops*, 2019, pp. 1–7.
- [36] X. Yang, C.-K. Wen, J. Yang, C.-J. Wang, S. Jin, and A. L. Swindlehurst, "Simple simultaneous localization and mapping through expectation propagation framework," *IEEE Trans. Commun.*, submitted for publication.
- [37] H. Wymeersch, G. Seco-Granados, G. Destino, D. Dardari, and F. Tufvesson, "5G mmWave positioning for vehicular networks," *IEEE Wireless Commun.*, vol. 24, no. 6, pp. 80–86, Dec. 2017.
- [38] G. Ghatak et al., "Beamwidth optimization and resource partitioning scheme for localization assisted mm-wave communications," *IEEE Trans. Commun.*, vol. 69, no. 2, pp. 1358–1374, Feb. 2021.
- [39] O. Igbafe, J. Kang, H. Wymeersch, and S. Kim, "Location-aware beam alignment for mmWave communications," 2020, *arXiv:* 1907.02197.
- [40] X. Yang, C.-K. Wen, S. Jin, A. Lee Swindlehurst, and J. Zhang, "Joint channel estimation and localization for cooperative millimeter wave systems," in *Proc. IEEE Int. Workshop Signal Process. Adv. Wireless Commun.*, 2020, pp. 1–5.
- [41] D. Shutin, W. Wang, and T. Jost, "Incremental sparse Bayesian learning for parameter estimation of superimposed signals," in *Proc. 10th Int. Conf. Sampling Theory Appl.*, 2013, no. 1, pp. 6–9.
- [42] D. Shutin and N. Schneckenburger, "Joint detection and super-resolution estimation of multipath signal parameters using incremental automatic relevance determination," 2015, arXiv:1503.01898.
- [43] D. Shutin and B. Vexler, "Sparse Bayesian learning with dictionary refinement for super-resolution through time," in *Proc. IEEE 7th Int. Workshop Comput. Adv. Multi-Sensor Adaptive Process.*, 2017, pp. 1–5.
- [44] T. L. Hansen, B. H. Fleury, and B. D. Rao, "Superfast line spectral estimation," *IEEE Trans. Signal Process.*, vol. 66, no. 10, pp. 2511–2526, May 2018.
- [45] A. Richter, "Estimation of radio channel parameters: Models and algorithms," Ph.D. dissertation, Ilmenau Univ. Technol., 2005.

- [46] B. H. Fleury, M. Tschudin, R. Heddergott, D. Dahlhaus, and K. I. Pedersen, "Channel parameter estimation in mobile radio environments using the SAGE algorithm," *IEEE J. Sel. Areas Commun.*, vol. 17, no. 3, pp. 434–450, Mar. 1999.
- [47] J. Salmi, A. Richter, and V. Koivunen, "Detection and tracking of MIMO propagation path parameters using state-space approach," *IEEE Trans. Signal Process.*, vol. 57, no. 4, pp. 1538–1550, Apr. 2009.
- [48] T. Jost, W. Wang, U. Fiebig, and F. Perez-Fontan, "Detection and tracking of mobile propagation channel paths," *IEEE Trans. Antennas Propag.*, vol. 60, no. 10, pp. 4875–4883, Oct. 2012.
- [49] X. Li, E. Leitinger, and F. Tufvesson, "Detection and tracking of multipath channel parameters using belief propagation," in *Proc. IEEE 54th Asilomar Conf. Signals, Syst.*, Comput., 2020, pp. 1083–1089.
- [50] C. M. Bishop, Pattern Recognition and Machine Learning (Information Science and Statistics). Secaucus, NJ, USA: Springer, 2006.
- [51] B. Nadler and A. Kontorovich, "Model selection for sinusoids in noise: Statistical analysis and a new penalty term," *IEEE Trans. Signal Process.*, vol. 59, no. 4, pp. 1333–1345, Apr. 2011.
- [52] F. Talebi and T. Pratt, "Model order selection for complex sinusoids in the presence of unknown correlated Gaussian noise," *IEEE Trans. Signal Process.*, vol. 63, no. 7, pp. 1664–1674, Jan. 2015.
- [53] E. Leitinger, S. Grebien, B. H. Fleury, and K. Witrisal, "Detection and estimation of a spectral line in MIMO systems," in *Proc. Asilomar*, 2020, pp. 1090–1095.
- [54] C.-K. Wen, C.-J. Wang, S. Jin, K.-K. Wong, and P. Ting, "Bayes-optimal joint channel-and-data estimation for massive MIMO with low-precision ADCs," *IEEE Trans. Signal Process.*, vol. 64, no. 10, pp. 2541–2556, May 2016.
- [55] J. Williams and R. Lau, "Approximate evaluation of marginal association probabilities with belief propagation," *IEEE Trans. Aerosp. Electron. Syst.*, vol. 50, no. 4, pp. 2942–2959, Oct. 2014.
- [56] Y. Bar-Shalom, F. Daum, and J. Huang, "The probabilistic data association filter," *IEEE Control Syst. Mag.*, vol. 29, no. 6, pp. 82–100, Dec. 2009.



Yu Han (Member, IEEE) received the B.S. degree in communications engineering from Hangzhou Dianzi University, Hangzhou, China, in 2012, and the M.S. and Ph.D. degrees in information and communications engineering from Southeast University, Nanjing, China, in 2015 and 2020, respectively. She was a Postdoctoral Fellow with the Singapore University of Technology and Design, Singapore, till 2022. Her research interests include extra large-scale MIMO and reconfigurable intelligent surface.



Shi Jin (Senior Member, IEEE) received the B.S. degree in communications engineering from the Guilin University of Electronic Technology, Guilin, China, in 1996, the M.S. degree from the Nanjing University of Posts and Telecommunications, Nanjing, China, in 2003, and the Ph.D. degree in information and communications engineering from Southeast University, Nanjing, China, in 2007. From June 2007 to October 2009, he was a Research Fellow with Adastral Park Research Campus, University College London, London, U.K. He is currently with the Faculty of

the National Mobile Communications Research Laboratory, Southeast University. His research interests include space time wireless communications, random matrix theory, and information theory. He was an Associate Editor for the IEEE TRANSACTIONS ON COMMUNICATIONS, IEEE TRANSACTIONS ON WIRELESS COMMUNICATIONS, IEEE COMMUNICATIONS LETTERS, and IET Communications. Dr. Jin and his coauthors have been awarded the 2011 IEEE Communications Society Stephen O. Rice Prize Paper Award in the field of communication theory and a 2010 Young Author Best Paper Award by the IEEE Signal Processing Society.



Xi Yang received the Ph.D. degree from the School of Information Science and Engineering, Southeast University, Nanjing, China, in 2021. His research interests include signal processing in wireless communications and the optimization of wireless multimedia networks



Chao-Kai Wen (Senior Member, IEEE) received the Ph.D. degree from the Institute of Communications Engineering, National Tsing Hua University, Hsinchu, Taiwan, in 2004. From 2004 to 2009, he was with Industrial Technology Research Institute, Hsinchu, Taiwan, and MediaTek Inc., Hsinchu, Taiwan, where he was engaged in broadband digital transceiver design. In 2009, he joined the Institute of Communications Engineering, National Sun Yat-sen University, Kaohsiung, Taiwan, where he is currently a Professor. His research focuses on the optimization

of wireless multimedia networks.



A. Lee Swindlehurst (Fellow, IEEE) received the B.S. and M.S. degrees in electrical engineering from Brigham Young University (BYU), Provo, UT, USA, in 1985 and 1986, respectively, and the Ph.D. degree in electrical engineering from Stanford University, Stanford, CA, USA, in 1991. From 1990 to 2007, he was with the Department of Electrical and Computer Engineering, BYU, where he was the Department Chair from 2003 to 2006. During 1996–1997, he held a joint appointment as a Visiting Scholar with Uppsala University, Uppsala, Sweden, and the Royal Institute

of Technology in Sweden. From 2006 to 2007, he was on leave as the Vice President of Research for ArrayComm LLC in San Jose, California. Since 2007, he has been a Professor with the Electrical Engineering and Computer Science Department, University of California Irvine, Irvine, CA, USA, where he was an Associate Dean of Research and Graduate Studies with the Samueli School of Engineering from 2013 to 2016. During 2014–2017, he was also a Hans Fischer Senior Fellow with the Institute for Advanced Studies, Technical University of Munich, Munich, Germany. In 2016, he was elected as a Foreign Member of the Royal Swedish Academy of Engineering Sciences. He has more than 300 publications in his research areas, which include array signal processing for radar, wireless communications, and biomedical applications. Dr. Swindlehurst was the inaugural Editor-in-Chief of the IEEE JOURNAL OF SELECTED TOPICS IN SIGNAL PROCESSING. He was the recipient of the 2000 IEEE W. R. G. Baker Prize Paper Award, 2006 IEEE Communications Society Stephen O. Rice Prize in the Field of Communication Theory, 2006 and 2010 IEEE Signal Processing Society's Best Paper Awards, and 2017 IEEE Signal Processing Society Donald G. Fink Overview Paper Award.